

Aus der Klinik für Herzchirurgie
der Heinrich-Heine-Universität Düsseldorf
Direktor: Univ.-Prof. Dr. med. Artur Lichtenberg

Dichloroacetate treatment to prevent the degeneration of
biological cardiovascular grafts

Dissertation
zur Erlangung des Grades eines Doktors der Medizin
der Medizinischen Fakultät der Heinrich-Heine-Universität Düsseldorf

vorgelegt von
Agunda Chekhoeva

2021

Als Inauguraldissertation gedruckt mit der Genehmigung der
Medizinischen Fakultät der Heinrich-Heine-Universität Düsseldorf

gez.:

Dekan: Herr Prof. Dr. med. Nikolaj Klöcker

Erstgutachter: Herr Prof. Dr. med. Alexander Assmann

Zweitgutachter: Herr Prof. Dr. med. Olaf Picker, MBA

For my mother who helped me in all things great and small.

Oral presentations:

VIII International Congress “Current trends of modern cardiothoracic surgery”; St. Petersburg, Russia, 21-23 June 2018

48th Annual Meeting of the German Society of Thoracic and Cardiovascular Surgery; Wiesbaden, Germany, 16-19 February 2019

Zusammenfassung

Herz-Kreislauf-Erkrankungen sind weltweit die häufigste Todesursache. Jedes Jahr sterben ungefähr 17,9 Millionen Menschen (World Health Organisation, 2017). Die bevorzugte Behandlung für Patienten mit fortgeschrittener Gefäßerkrankung ist die Verwendung von Gefäßtransplantaten, um enge oder verschlossene Gefäße zu ersetzen oder zu umgehen. Autologe Gefäße wie die *Vena saphena* und die *A. thoracica interna* bleiben die ideale Ressource, aber nicht alle Patienten verfügen über ausreichende oder gesunde autologe Transplantate für die Gefäßtransplantation. Gegenwärtige kommerzielle Gefäßtransplantate mit kleinem Durchmesser weisen einen Mangel aufgrund einer fortschreitenden *in-vivo*-Thrombose und Verkalkung auf. *Tissue engineer*te Gefäßprothesen, insbesondere dezellularisierte Implantate, stellen eine neue Quelle für Gefäßprothesen dar, die im Vergleich zu Transplantaten mit klinischem Standard eine verbesserte Lebensfähigkeit, Biokompatibilität und biologische Aktivität aufweisen können.

Ein Hauptbestandteil des Transplantatversagens ist die frühe Neointima-Hyperplasie, die hauptsächlich durch die Proliferation von Myofibroblasten verursacht wird und zu einer fortschreitenden *in-vivo*-Degeneration führt (Liu et al., 2013). Deuse et al. haben gezeigt, dass die systemische Anwendung der Apoptose-unterstützenden Substanz Dichloroacetat (DCA) in verschiedenen Groß- und Kleintier-Modellen zu einer verringerten neointimalen Hyperplasie bei intimal geschädigten Arterien führt. Gleichzeitig wurde die autologe Endothelialisierung der geschädigten Gefäßabschnitte nicht verhindert (Deuse et al., 2014). Eine unkontrollierte Proliferation der Myofibroblasten und der glatten Muskelzellen wird durch DCA verhindert, was zu erhöhtem oxidativem Stress und Zellapoptose führt. Da die Proliferation von Myofibroblasten ein Hauptbestandteil der Degeneration verletzter nativer Gefäße ist und DCA diesen Mechanismus hemmen kann, ist anzunehmen, dass die Proliferation von Myofibroblasten in biologischen kardiovaskulären Implantaten ebenfalls verhindert werden kann. Detergenzien-basierte dezellularisierte Spenderratten-Aortentransplantate (n=22) wurden mit Fibronektin (FN) (50 µl/ml, 24 h) beschichtet und in die infrarenale Aorta der Empfängerratten implantiert. Ratten in der DCA-Gruppe (n=12) erhielten DCA über Trinkwasser (0,75 g/dl), während Ratten ohne DCA-Behandlung als Kontrolle dienten (n=10). Nach zwei und acht Wochen wurden die Transplantate explantiert und durch Histologie und Immunfluoreszenz untersucht. Die systemische DCA-Behandlung hemmte die Neointima-Bildung, was zu einem signifikant verringerten Verhältnis von Intima zu Media führte (0.87 ± 0.06 vs. 1.97 ± 0.24 ; $p < 0.001$). Darüber hinaus war nach acht Wochen die Neointima-Verkalkung, die anhand eines etablierten Von-Kossa-Färbungsscores bewertet wurde, in der DCA-Gruppe signifikant verringert (anastomotic regions: A1: 0.2083 ± 0.1039 vs. 0.8500 ± 0.2927 , $p < 0.05$; B2: 0.2083 ± 0.1343 vs. 0.8000 ± 0.2128 , $p < 0.05$; / non-anastomotic regions A2: 0.0416 ± 0.0416 vs. 0.8000 ± 0.2865 , $p < 0.01$; B1: 0.4167 ± 0.1694 vs. 1.200 ± 0.2575 , $p < 0.05$). Nach acht Wochen waren explantierte Transplantate in beiden Gruppen vollständig von einer Endothelzellschicht bedeckt, und in beiden Gruppen erwiesen sich Entzündungszellmarker (CD3, CD68) als negativ.

Die systemische DCA-Behandlung reduzierte die Neointima-Bildung bei dezellularisierten arteriellen Transplantaten und ermöglichte gleichzeitig eine schnelle Reendothelialisierung der Implantate. Darüber hinaus schützte DCA die Transplantate vor Verkalkung.

Abstract

Cardiovascular diseases are the leading cause of death globally, taking an estimated 17.9 million lives each year (World Health Organisation, 2017). The favoured treatment for patients with advanced vascular disease is the use of vascular grafts to replace or bypass narrow or occluded vessels. Autologous vessels such as the saphenous vein and the internal thoracic artery remain the ideal resource, but not all patients have sufficient or healthy autologous grafts for vascular grafting. Present small-diameter commercial vascular grafts have deficiency due to progressive *in vivo* thrombosis and calcification. Tissue-engineered vascular prostheses, in particular decellularized implants, represent a new source of vascular prostheses that carry the potential to feature improved viability, biocompatibility and biological activity as compared to clinical standard grafts.

A major component of graft failure is early neointima hyperplasia mainly driven by myofibroblast proliferation resulting in progressive *in vivo* degeneration (Liu *et al.*, 2013). Deuse *et al.* have shown that the systemic application of the apoptosis-supporting substance dichloroacetate (DCA) in various large and small animal models leads to reduced neointimal hyperplasia on intimal damaged arterial vessels. At the same time, the autologous endothelialization of the damaged vascular sections was not prevented (Deuse *et al.*, 2014). Uncontrolled myofibroblast and smooth muscle cell proliferation are prevented by DCA causing enhanced oxidative stress leading to cell apoptosis. Since myofibroblast proliferation is a major component of the degeneration of injured native vessels, and DCA can inhibit this mechanism, we hypothesize that myofibroblast proliferation in biological cardiovascular implants may be prevented likewise. Detergent-decellularized donor rat aortic grafts (n=22) were surface-coated with fibronectin (FN) (50 µl/ml, 24 h incubation) and implanted via anastomoses to the infrarenal aorta of the recipient rats. Rats in the DCA group (n=12) received DCA via drinking water (0.75 g/dl), while rats without DCA treatment served as controls (n=10). After 2 and 8 weeks, the grafts were explanted and examined by histology and immunofluorescence. Systemic DCA treatment inhibited neointima formation, resulting in a significantly reduced intima-to-media ratio (0.87 ± 0.06 vs. 1.97 ± 0.24 ; $p < 0.001$). In addition, at 8 weeks, neointima calcification, as assessed by an established von Kossa (VK) staining-based score, was significantly decreased in the DCA group (anastomotic regions: A1: 0.2083 ± 0.1039 vs. 0.8500 ± 0.2927 , $p < 0.05$; B2: 0.2083 ± 0.1343 vs. 0.8000 ± 0.2128 , $p < 0.05$; / non-anastomotic regions A2: 0.0416 ± 0.0416 vs. 0.8000 ± 0.2865 , $p < 0.01$; B1: 0.4167 ± 0.1694 vs. 1.200 ± 0.2575 , $p < 0.05$). After 8 weeks, explanted grafts in both groups were lumenally completely covered by an endothelial cell layer and in both groups, inflammatory cell markers (CD3, CD68) proved negative.

Systemic DCA treatment reduced neointima formation on decellularized arterial grafts, while allowing for rapid reendothelialization of the implants. Furthermore, DCA protected the grafts from calcification.

Abbreviations

ANOVA	Analysis of variance
ATP	Adenosintriphosphat
BSA	Bovines serum albumin
CD	Cluster of differentiation
CVD	Cardiovascular disease
DAPI	Diamidinophenylindol
DCA	Dichloroacetate
ECM	Extracellular matrix
EDTA	Ethylendiamintetraacetat
FDA	Food and drug administration
FN	Fibronectin
HE	Hematoxylin-eosin
IH	Intima hyperplasia
MI	Myocardial infarction
MMP	Matrix-metallo-proteinase
PAH	Pulmonary arterial hypertension
PBS	Phosphate buffered saline
PCL	Polycaprolactone
PDGF	Platelet derived growth factor
PDH	Pyruvate dehydrogenase
PDK2	Pyruvate dehydrogenase kinase 2
PGA	Poly-glycolic acid
PLA	Poly-lactic acid
PTFE	Polytetrafluoroethylene
SDF1 α	Stromal derived factor 1 alpha
SEM	Standard error of the mean
TE	Tissue engineering
TEVG	Tissue engineered vascular graft
TRIS	Tris(hydroxymethyl)-aminomethan
VK	Von Kossa
VSMC	Vascular smooth muscle cell
vWF	von Willebrand Factor
α SMA	alpha-Smooth muscle actin

Table of Contents

1. Objectives	1
1.1 Cardiovascular tissue engineering	1
1.1.1 Scaffold-based vascular tissue-engineering methods	2
1.1.2 Self-assembled TEVG	5
1.1.3 Decellularized natural matrices	5
1.2 Recellularization of TEVG	6
1.3 Dichloroacetate to prevent intimal hyperplasia	7
1.4 Study aim	10
2. Materials and Methods	11
2.1 Materials	11
2.1.1 Chemicals	11
2.1.2 Antibodies	13
2.1.3 Solutions	13
2.1.4 Devices and materials	15
2.1.5 Software	17
2.2 Study design	18
2.3 Surgical procedure	19
2.3.1 Donor operation	19
2.3.2 Decellularization	19
2.3.3 Graft coating with fibronectin	20
2.3.4 Recipient procedure	20
2.3.5 Graft explantation	21
2.4 Histology	21
2.4.1 Hematoxylin-eosin stain	22
2.4.2 Von Kossa stain	22
2.4.3 Movat pentachrome stain	23
2.4.4 Immunofluorescence stain	24
2.4.5 <i>In Situ</i> zymography	25
2.5 Morphological characterization of explanted grafts	26
2.5.1 Neointima formation	26
2.5.2 Media repopulation	27
2.5.3 Calcification	28
2.5.4 MMP Activity	29
2.5.5 Statistical analysis	29
2.6 Ethics vote and animal experiment approval	30
3. Results	31
3.1 Operative results	31
3.2 Neointima and media formation	31
3.3 Neointima and media calcification	38
3.4 In situ zymography	41
4. Discussion	42
4.1 Influence of dichloroacetate on graft recellularization	44
4.2 Influence of dichloroacetate on intimal hyperplasia	44

4.3	Influence of dichloroacetate on graft calcification	45
4.4	Limitations	46
4.5	Perspectives	46
5.	<i>References</i>	47
	<i>Acknowledgment</i>	53

1. Objectives

Cardiovascular disease (CVD) is the number one killer in the United States (Virani *et al.*, 2020). It includes cerebrovascular disease, coronary heart disease, peripheral artery disease, atherosclerosis, angina pectoris, and congenital cardiovascular defects. In the pediatric population, congenital heart disease is the most common malformation occurring in newborns and the most frequent cause of infant death (America *et al.*, 2020). The majority of CVDs and some congenital heart diseases are associated with ischemia caused by blood flow obstruction or stenosis. Blood flow obstruction in the coronary circulation can trigger myocardial infarction (MI), while blood flow obstruction or stenosis in congenital heart disease leads to cyanosis or blood circulation disorder.

A clinical similarity between CVD and congenital heart disease is the need for revascularization procedures. Native vessels are the ideal source for revascularization. However, autologous grafts are not always possible due to limited availability. Synthetic vascular grafts such as PTFE (Gortex, W.L. Gore & Associates, Newark, DE) and polyethylene terephthalate (Dacron, Dupont, Wilmington, DE) have limitations such as thrombogenicity, risk of infection, aneurysm formation, and the need for anticoagulation (Udelsman, Maxfield and Breuer, 2013). Biological grafts such as dialdehyde starch (Artegraft bovine carotid artery graft, Johnson and Johnson) and glutaraldehyde (Biograft human umbilical vein graft, Meadox Medical) were clinically used, and both were found to undergo structural changes after implantation, including vessel wall calcification and aneurysmal degeneration (Thomas *et al.*, 1991).

In pediatric patients, synthetic and biological prostheses are limited by their lack of growth potential, resulting in delayed treatment and graft oversizing, both of which increase complications (Alexi-Meskishvili *et al.*, 2000).

Tissue-engineered vascular grafts (TEVGs) are a graft source that may overcome the limitations of standard clinical grafts. An ideal artificial vascular graft closely mimics the natural vessel and should be resistant to thrombosis, inflammation, and neointimal proliferation (Ravi and Chaikof, 2010).

1.1 Cardiovascular tissue engineering

The first synthetic grafts were introduced in the 1950s following surgical complications associated with harvesting vessels, a frequent shortage of allogeneic grafts, and immunological rejection of large animal-derived vessels (Kurniawan, 2019). Since the

1950s, synthetic vascular grafts were clinically used as large-diameter conduits (Song *et al.*, 2019). But complications arose when they were used for smaller vessels (Cartmill, 1987).

The scientific progress during the last few decades has led to our current understanding of vascular biology and tissue engineering (TE) and to innovative solutions to key challenges. As shown in Fig. 1, TE today primarily revolves around several different approaches to graft synthesis: scaffold-based methods, self-assembled TEVGs, and decellularized natural matrices (Simbara *et al.*, 2017).

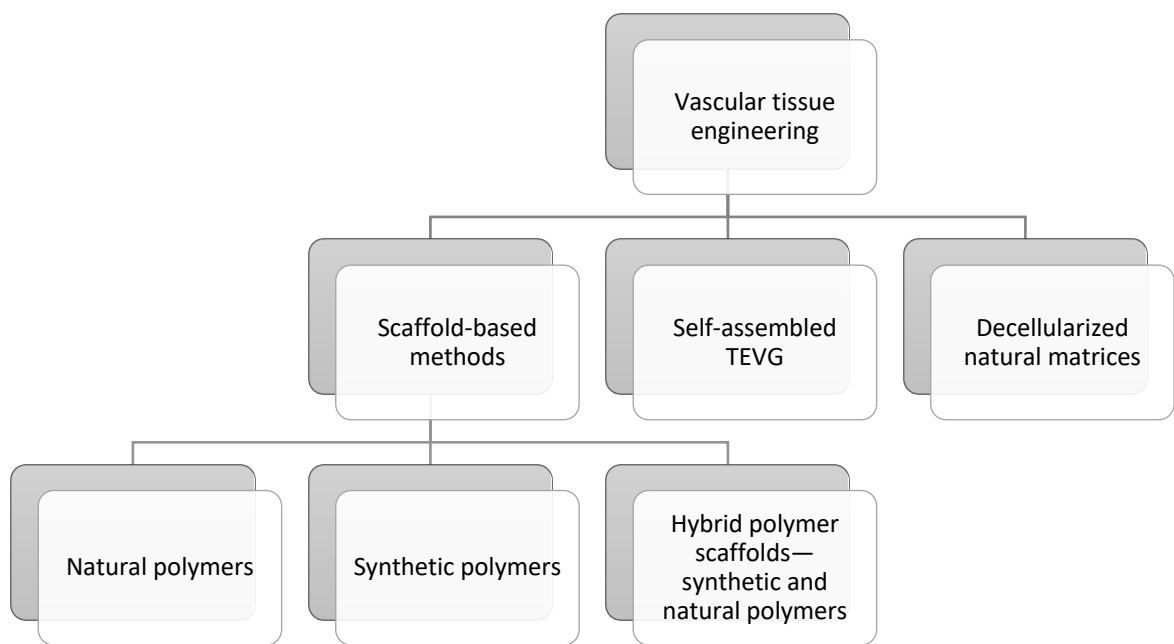


Fig. 1 TEVG method designs.

1.1.1 Scaffold-based vascular tissue-engineering methods

Vascular tissue-engineered scaffolds are made from a range of synthetic and natural materials and manufactured using several different techniques (Pashneh-Tala, MacNeil and Claeysens, 2016). The concept of combining cells with a scaffold is central to most tissue-engineering approaches. Scaffold-based vascular TE aims to provide a template of the required construct.

Natural polymers represent a rational choice for designing scaffolds for TE, offering potentially improved biocompatibility without inflammation or toxicity (Matsuzaki *et al.*, 2019). Fibrin (Kaplan *et al.*, 2017), elastin (McKenna *et al.*, 2008), silk fibroin (Van Uden *et al.*, 2019)(Lovett *et al.*, 2010)(Marelli *et al.*, 2010), and collagen (Copes *et al.*, 2019) are the most studied natural polymers for application in vascular TE. Natural scaffolds allow better cell attachment, but they are susceptible to enzymatic degradation and have poor mechanical properties; these issues can be overcome by various approaches, including crosslinking. Additionally, vascular cell breakdown and remodeling may be impeded by the high degree of compaction of natural polymer scaffolds (Pashneh-Tala, MacNeil and Claeyssens, 2016).

Collagen is the major component of the extracellular matrix (ECM). It is mainly secreted by smooth muscle cells in the media and fibroblasts in the adventitia. Currently, 29 different types of collagen have been identified (Gelse, Poschl and Aigner, 2003). Type I collagen is one of the major biopolymers used in scaffold technology. Because of their weak antigenic, inflammatory, and cytotoxic responses together with their good biocompatibility, collagen gels are suitable substrates for cell culture (Couet, Rajan and Mantovani, 2007).

Significant success has been achieved using **fibrin** as a scaffold material (Pashneh-Tala, MacNeil and Claeyssens, 2016). It can be produced from polymerized fibrinogen isolated from a patient's own blood plasma. Consequently, fibrin-based scaffolds do not cause adverse inflammatory reactions (Assmann *et al.*, 2013).

Elastin is especially found in the artery walls. In several studies, a triple-layered vessel constructed from elastin fibers, collagen fibrils (Koens *et al.*, 2010), silk fibroin, collagen, elastin, and polycaprolactone (PCL) (McClure, Simpson and Bowlin, 2012) was used.

Silk fibroin also has potential as a scaffold material for TEVGs. Silk from the silkworm, *Bombyx mori*, has been used as biomedical suture material (Altman *et al.*, 2003). It offers strong mechanical properties together with biocompatibility and slow degradation *in vivo* (Lovett *et al.*, 2010), and it is compatible with several manufacturing processes (Pashneh-Tala, MacNeil and Claeyssens, 2016).

Biodegradable synthetic polymers offer several advantages over other materials for developing scaffolds in TE. The main advantage of synthetic polymer-based TEVGs is their controllability arising from their thermal and mechanical properties (Alizadeh-Osgouei, Li and Wen, 2019). The relatively low cost of producing synthetic polymer scaffolds coupled with the ability to tune various properties associated with them has been key to their extensive use and offers excellent potential for the future.

Commonly used synthetic polymers are PCL, polylactic acid (PLA), and polyglycolic acid (PGA).

As one of the most popular biodegradable scaffolds, **PGA** has been commonly used in constructing engineered vessels due to its good biocompatibility (Niklason *et al.*, 2001). A major advantage of PGA is its suitable degradation rate, which matches the kinetics of new tissue formation (Wang *et al.*, 2010). By using PGA scaffolds, Niklason *et al.* constructed the first autologous vascular graft and implanted it in the arterial system (Niklason *et al.*, 1999). In another study, Hollinger 1983, suggests that this polymer is sufficiently biocompatible, although certain studies suggest otherwise (Gunatillake, Adhikari and Gadegaard, 2003).

Polylactic acid is one of the most well-researched and commonly used polymers for biodegradable medical applications (Alizadeh-Osgouei, Li and Wen, 2019). It is more hydrophobic than PGA and is more resistant to hydrolytic attack (Gunatillake, Adhikari and Gadegaard, 2003). It degrades to form lactic acid, which is normally present in the body. This acid then enters the tricarboxylic acid cycle and is excreted as water and carbon dioxide. Polylactic acid is suitable for a wide range of applications in medical science due to its biodegradability and biocompatibility (Alizadeh-Osgouei, Li and Wen, 2019). Polyesters are the most used polymers in bone TE.

Polycaprolactone is another saturated aliphatic biodegradable polyester used in developing TE scaffolds (bone, cartilage, and cardiovascular) and other biomedical applications (sutures, wound dressings, contraceptive devices, and dental materials) (Song *et al.*, 2018).

Hybrid scaffolds are based on both natural and synthetic polymers. Coating synthetic polymer scaffolds with collagen, FN, and gelatin improves their biocompatibility and cell adhesion (Wise *et al.*, 2011)(Koch *et al.*, 2010)(Tillman *et al.*, 2009). These scaffolds are believed to improve biocompatibility and biochemical properties due to their potential to exploit the best of both synthetic and natural polymer scaffold systems in producing TEVGs (Pashneh-Tala, MacNeil and Claeysens, 2016). *In vivo* experiments were performed during the last decade that demonstrated the feasibility of the hybrid approach (Carrabba and Madeddu, 2018). The need for long conditioning times, particularly for long periods of *in vitro* culture to generate robust constructs, is the main limitation associated with using hybrid scaffolds.

1.1.2 Self-assembled TEVG

Despite the improvements achieved in fabricating TEVGs based on scaffolds, some researchers tested the self-assembled TEVGs (Norotte *et al.*, 2009)(Gauvin *et al.*, 2010)(Kelm *et al.*, 2010)(Bourget *et al.*, 2012). This approach was pioneered in the form of sheet-based TE but now includes other methods, such as cell-sheet assembly, microtissue aggregation, and cell printing (Carrabba and Madeddu, 2018).

The first successful scaffold-free concept was introduced by L'Heureux *et al.* in a canine model. The process involved producing sheets of cells, where single-cell sheets were wrapped in a multistep process around a mandrel, forming the tubular structure of a vascular graft (L'Heureux *et al.*, 1998). The resulting tissue displayed good functionality, good mechanical properties *in vivo*, and the ability to produce an ECM containing types I, III, and IV collagens as well as laminin, FN, and chondroitin sulfates, which are needed to structurally support the vessel (L'Heureux *et al.*, 1998). Engineered vessels produced using this method are currently used in clinical studies for hemodialysis access (Lifeline, Cytograft Tissue Engineering Inc., Novato, CA) (Wystrychowski *et al.*, 2014).

Using TE by self-assembly is limited in terms of long production times and the geometries that the graft can assume. The possibility of overcoming this limitation and building patient-specific vascular grafts using 3D bioprinting was recently proposed; however, this remains to be confirmed.

1.1.3 Decellularized natural matrices

Decellularization is a promising approach used in biomedical engineering to isolate the ECM, leaving an ECM scaffold of the original tissue to produce small- and large-diameter vascular grafts and artificial organs. Various decellularized vessels seeded with cells have been evaluated in animal studies, and the first vascular grafts were developed in the 1960s using animal tissue (Rosenberg *et al.*, 1966). A literature review revealed that many experimental groups reported the decellularization of the human umbilical cord artery (Mallis *et al.*, 2014)(Rodríguez-Rodríguez *et al.*, 2018), femoral artery (Wilshaw *et al.*, 2012), pulmonary artery (Hopkins *et al.*, 2014) and internal thoracic artery (Jones *et al.*, 2014)(Kajbafzadeh *et al.*, 2017), achieving good results in terms of structural and mechanical characteristics.

Numerous decellularization techniques were developed, including chemical (Akbari Zahmati *et al.*, 2017), enzymatic (Chen *et al.*, 2017), and mechanical (Gilpin and Yang,

2017) treatment methods. An evaluation of these strategies focused on the removal of cells and genetic material followed by the maintenance of structural proteins. Physical methods include freeze/thaw cycles, high hydrostatic pressure, and supercritical carbon dioxide. Although these are typically less damaging to the tissue structure, they are rarely sufficient by themselves, and they fail to meet the requirements for immunogenicity. Biological (e.g., enzymes) and chemical (e.g., surfactants, acids, and bases) techniques tend to damage the cell membrane, break down intra- and extracellular bonds and may not completely remove all cellular debris when used alone (Gilpin and Yang, 2017). Thus, the ideal technique varies according to the combination of the two treatments and should be tissue specific.

Commercially available small-caliber vascular grafts, Artegraft (Lindsey *et al.*, 2018), Solcograft (Nemes *et al.*, 1985), and ProCol (Schmidli *et al.*, 2004), which were based on decellularized bovine blood vessels, and SynerGraft model 100 (Brown *et al.*, 2011), which was derived from decellularized bovine ureter, have limited performances due to their lack of cellularity on implantation (Lin *et al.*, 2018).

Decellularized pulmonary and aortic heart valves are used in clinical practice. At the Hannover Medical School between May 2011 and June 2017, aortic and pulmonary valve homografts were harvested under sterile conditions from cadavers, brain-dead multiorgan donors, or transplant patients (domino hearts). After decellularization was performed by detergent treatment of the homografts (Bobylev *et al.*, 2019), a double semi-lunar valve replacement was performed in selected cases with excellent early to midterm results (Boethig *et al.*, 2019). True long-term durability of decellularized human heart valves and vascular grafts can only be expected if recellularization occurs to enable elastic fibers, the collagen matrix structure, proteoglycans, and other extracellular proteins to continuously regenerate.

1.2 Recellularization of TEVG

The disadvantages of cell-free decellularized grafts are the risk of incomplete endothelialization and early intimal hyperplasia *in vivo* (Lin *et al.*, 2018). Endothelialization is necessary to overcome immune-response- or thrombosis-mediated graft failure. Recent studies focused on surface treatment of artificial and biological vascular grafts with bioactive agents and multipotent stem cells to accelerate the *in vivo* adhesion of recipient cells. The ECM, including stromal-cell-derived factor 1 alpha (SDF-1 α) (Sugimura *et al.*, 2020), laminin (Toshmatova *et al.*, 2019), FN (Assmann *et al.*, 2013), and heparin (Cai *et al.*, 2009), is known to affect the migration, function, and homeostasis of the cells. Cell seeding plays

an important role in the maintenance of vascular graft patency and is largely dependent on the complexity of the cell sheet, tissue, or organ of interest.

Fibronectin was first isolated from blood more than 60 years ago (To and Midwood, 2011). There are two general sources of FN: the plasma form of FN that is synthesized by hepatocytes and secreted into blood, where it circulates in a compact conformation and, on tissue injury, is incorporated into fibrin clots to affect platelet function and mediate hemostasis, and the cellular form of FN that is secreted locally by cells as they migrate into the clot to reconstitute damaged tissue (Lisa M. Maurer, Ma and Mosher, 2015) (To and Midwood, 2011).

Fibronectin is a group of glycoproteins of cell surfaces, blood plasma, and connective tissue that promotes cellular adhesion and migration. It is present in all tissues and throughout all stages of life, is secreted as a large ECM glycoprotein with a mass of 230–270 kDa, and is assembled via a cell-mediated process (Mosher, 1993). FN is a multidomain protein and comprises three modules of repeating units (Schwarzbauer and DeSimone, 2011). The modules are organized into functional domains that are resistant to proteolysis (Potts, 1975).

Due to the failure of endothelial-cell-seeded vascular prostheses, some research groups pretreated their grafts with FN to increase endothelial cell adhesion (Assmann *et al.*, 2013)(Ramalanjaona *et al.*, 1986)(Assmann *et al.*, 2017). Polytetrafluoroethylene (PTFE) vascular graft incubated with FN-tagged iodine-125 was tested in *in vitro* and *in vivo* models (Ramalanjaona *et al.*, 1986). This study shows that binding of FN onto a PTFE graft is concentration dependent. A concentration of 50–250 µg/ml FN led to an increase in binding with a PTFE prosthesis, while doubling the concentration (250–500 µg/ml) resulted in only a 33.4% improvement in binding rather than the expected 52.4%.

Another *in vivo* study was performed that used 50 µg/ml FN as a luminal and adventitial coating agent in decellularized vascular conduits (Assmann *et al.*, 2013). FN was present for up to eight weeks in the systemic circulation and induced accelerated medial graft repopulation in the absence of an inflammatory reaction. FN showed good biocompatibility without thrombogenicity. Moreover, FN not only accelerates neointima formation but also aggravates IH, so that different strategies are necessary to overcome this issue.

1.3 Dichloroacetate to prevent intimal hyperplasia

Intimal hyperplasia (IH) is the thickening of the tunica intima of a blood vessel. Several studies were performed to investigate the mechanism and prevention of IH. Wang

et al. demonstrated for the first time that controlling mitochondrial fission can reduce platelet-derived growth factor (PDGF)-induced vascular smooth muscle cells (VSMC) migration and pathological IH (Wang *et al.*, 2015).

Deuse et al. showed that mitochondrial metabolism and its regulatory key enzyme, pyruvate dehydrogenase kinase 2 (PDK2), play an important role in myointima formation. Throughout VSMC proliferation, the phosphorylation of pyruvate dehydrogenase (PDH) with a regulated flow of pyruvate into the mitochondria was observed. Increased proliferation of ECM caused IH (Deuse *et al.*, 2014).

Pharmacological or genetic inhibition of PDK2 and target mitochondrial therapy may be a novel strategy for preventing proliferative neointimal hyperplasia and restenosis.

Dichloroacetate is a small water-soluble acid molecule with a mass of 150 Da, which allows it to achieve 100% bioavailability (Duan *et al.*, 2013). Both oral and parenteral DCA formulations are available for clinical use, and DCA is metabolized in the liver. After higher doses, such as therapeutic doses, DCA has slower clearance from the body. This effect appears to plateau, and DCA serum levels do not continue to rise with ongoing use (Michelakis, Webster and Mackey, 2008). DCA-treated rats showed no evidence of severe hematologic, liver, renal, blood, or cardiac toxicity. Side effects of DCA include common gastrointestinal effects, and treatment is limited in cases of peripheral neuropathy (Kho *et al.*, 2019).

Dichloroacetate is a PDH activator and a mitochondrial pyruvate dehydrogenase kinase inhibitor used in treating acute and chronic lactic acidosis (Bonnet *et al.*, 2007) and inherited disorders of mitochondrial metabolism. Due to its anti-Warburg effect, it has been studied for a long time, especially in cancer research as an anticancer drug (Zhao *et al.*, 2019) (Tataranni and Piccoli, 2019). Because of a lack of evidence that DCA is effective in fighting cancer, it has not been approved by the Food and Drug Administration (FDA) for cancer treatment ('Complementary Approaches : Dichloroacetate (DCA)', 2020).

Because DCA is selective for the pulmonary circulation, two studies were performed to prevent and reverse pulmonary hypertension in rats (Michelakis *et al.*, 2015)(McMurtry *et al.*, 2004). It was shown that a low dose of 0.75 g/L is probably a threshold dose, minimally affecting hemodynamics. A high dose of 7.5 g/L had only minimal additional effects compared with 0.75 g/L. This study presented mitochondria-dependent apoptosis as a potential target for therapy and DCA as an effective and selective treatment for pulmonary arterial hypertension (PAH) (McMurtry *et al.*, 2004).

Recent studies have shown that DCA acts as a potential vasoprotective agent by inhibiting PDK2 and promoting revascularization of blood vessels (Deuse *et al.*, 2014). Due

to PDK2 blockade, DCA prevented mitochondrial membrane potential hyperpolarization, facilitated apoptosis, and reduced myointima formation in injured human mammary and coronary arteries, rat aortas, rabbit iliac arteries, and swine coronary arteries, but it did not prevent luminal re-endothelialization (Deuse *et al.*, 2014).

1.4 Study aim

The overarching aim of the current project was to examine the potential of systemic DCA treatment to prevent neointimal hyperplasia and progressive degeneration of decellularized aortic grafts coated with FN *in vivo*.

Systemic DCA treatment was conducted by addition to the drinking water, while untreated animals served as controls. The comparative readout focused on early autologous repopulation of the prostheses after implantation and signs of inflammatory reaction as well as degenerative processes in the grafts. Evaluation methods included histology and immunohistology.

Based on previous data, we expected severe intimal myofibroblast hyperplasia on biological cardiovascular grafts to be diminished by DCA treatment. In decellularized grafts coated with FN, IH should occur; however, the beneficial effect of DCA should be observed. Moreover, signs of advanced calcification were examined.

In this project, the following questions were investigated:

1. Does systemic DCA treatment influence graft recellularization?
2. Does systemic DCA treatment prevent IH?
3. Does systemic DCA treatment prevent graft calcification?

2. Materials and Methods

2.1 Materials

2.1.1 Chemicals

Acetic acid	Carl Roth, Karlsruhe, Germany
Aceton	Merck KGaA, Darmstadt, Germany
Acid fuchsin	Carl Roth, Karlsruhe, Germany
Albumin fraction V	Carl Roth, Karlsruhe, Germany
Alcian blue	Sigma-Aldrich Chemie, Taufkirchen, Germany
Alcohol	Central Pharmacy, HHU Duesseldorf, Germany
Ammonium hydroxide	Carl Roth, Karlsruhe, Germany
Betadine	Mundipharma, Limburg an der Lahn, Germany
Bovines serum albumin	Sigma-Aldrich Chemie, Taufkirchen, Germany
Brilliant crocein R	Waldeck GmbH & Co. KG, Münster, Germany
Calciumchlorid dihydrat	Merck KGaA, Darmstadt, Germany
DQ Gelatin	Thermo Fisher Scientific, Waltham, Massachusetts, USA
Dichloroacetat	Sigma-Aldrich Chemie, Taufkirchen, Germany
DNase	Sigma-Aldrich Chemie, Taufkirchen, Germany
Iron (III) chloride	Sigma-Aldrich Chemie, Taufkirchen, Germany
Eosin B	Sigma-Aldrich Chemie, Taufkirchen, Germany
Fibronectin (FN)	Sigma-Aldrich Chemie, Taufkirchen, Germany
Formaldehyde	Carl Roth, Karlsruhe, Germany
Formalin	Carl Roth, Karlsruhe, Germany

Hematoxylin	Thermo Fisher Scientific, Waltham, Massachusetts, USA
Heparin	Rotexmedica, Trittau, Germany
Hydrochloric acid	Carl Roth, Karlsruhe, Germany
Iod	Carl Roth, Karlsruhe, Germany
Isoflurane	Actaris, Langenfeld, Germany
Isopropranol	Merck KGaA, Darmstadt, Germany
Kaliumiodid	Carl Roth, Karlsruhe, Germany
Kernechtrot-aluminum sulfate	Carl Roth, Karlsruhe, Germany
Nail polish	Dm-Drogeriemarkt, Karlsruhe, Germany
Penicillin streptomycin solution	Invitrogen Carlsbad, USA
Picric acid	VWR International GmbH- Darmstadt, Germany
Phosphate buffered saline	Sigma-Aldrich Chemie, Taufkirchen, Germany
Phosphotungstic acid	Sigma-Aldrich Chemie, Taufkirchen, Germany
Roti-histokitt mounting medium for histology	Carl Roth, Karlsruhe, Germany
Safran de Getinai	Waldeck GmbH & Co. KG, Münster, Germany
Silver nitrate	Carl Roth, Karlsruhe, Germany
Sodium azide	Sigma-Aldrich Chemie, Taufkirchen, Germany
Sodium carbonate	Merck KGaA, Darmstadt, Germany
Sodium chloride	Carl Roth, Karlsruhe, Germany
Sodium deoxycholate	Sigma-Aldrich Chemie, Taufkirchen, Germany
Sodium dodecyl sulfate	Carl Roth, Karlsruhe, Germany
Solution Ringer	Fresenius, Bad Homberg, Germany
Sodium thiosulfate	Sigma-Aldrich Chemie, Taufkirchen, Germany
Titriplex III	Merck KGaA, Darmstadt, Germany
Tris (hydroxymethyl) aminomethane hydrochloride	Carl Roth, Karlsruhe, Germany

Triton X-100	Sigma-Aldrich Chemie, Taufkirchen, Germany
Tween 20	Merck KGaA, Darmstadt, Germany
Vectashield antifade mounting medium with Dapi	Vector labs Peterborough, England
Xylene	VWR International GmbH - Darmstadt, Germany

2.1.2 Antibodies

Primary antibodies

Anti-von-Willebrand-Factor	Dako, Hamburg, Germany
Anti-Alpha-smooth muscle actin	Sigma-Aldrich Chemie, Taufkirchen, Germany
Anti-CD3	Sigma-Aldrich Chemie, Taufkirchen, Germany
Anti-CD68	Abcam, Cambridge, England

Secondary antibodies

Alexa488 anti-rabbit	Invitrogen Carlsbad, USA
Alexa546 anti-mouse	Invitrogen Carlsbad, USA

2.1.3 Solutions

Decellularization

Decellularization solution 0	1g Penicillin/Streptomycin 100 ml PBS
Decellularization solution 1	5 g sodium dodecyl sulfate 5 g sodium deoxycholate 0,5 g sodium azide 1000 ml distilled water
Decellularization solution 2	0,032 g DNase 14 ml PBS

Hematoxylin-eosin stain

Eosin solution	1 g eosin 100 ml distilled water
----------------	-------------------------------------

4-5% Acetic acid	100 ml 100% alcohol 200 µl glacial acetic acid 10 ml glacial acetic acid 200 ml water
Von Kossa stain	
5% Silver nitrate solution	10 g silver nitrate 200 ml distilled water
5% Sodium thiosulfate solution	10 g sodium thiosulfate 200 ml distilled water
Sodium carbonat formaldehyde solution	10 g sodium carbonat 50 ml formaldehyde 200 ml distilled water
Movat pentachrome stain	
Alkaline alcohol	40 ml 30% ammonium hydroxide 400 ml 96% alcohol
Bouin's solution	100 ml 40% formaldehyde 20 ml 100% acetic acid 300 ml picric acid
1% Alcian blue solution	2 g alcian blue 200 ml distilled water
Weigert's iron hematoxylin	40 ml iron chloride solution 20 ml iod solution 60 ml alcoholic hematoxylin solution
Iron chloride solution	12,4 g iron chloride 5 ml 35% hydrochloric acid 500 ml distilled water
Iodine solution	10 g iodine 20 g potassium iodide 500 ml distilled water
2% Alcoholic hematoxylin solution	10 g hematoxylin 500 ml 96% alcohol
Crocein scarlet (stock solution)	20 ml acid fuchsin 80 ml brilliant crocein R
Brilliant crocein R	4 g brilliant crocein R 400 ml distilled water

Acid fuchsin (stock solution)	0,5 g acid fuchsin 2,5 ml 100% glacial acetic acid 500 ml distilled water
5% Phosphotungstic acid solution	25 g phosphotungstic acid 500 ml distilled water
1% Glacial acetic acid	5 ml 100% acetic acid 500 ml distilled water
Alcoholic safran solution	12 g safran de getinai 200 ml 100% alcohol
5% Sodium thiosulfate	10 mg sodium thiosulfate 200 ml distilled water

Immunofluorescence stain

0,1% Tween	500 µl tween 20 500 ml PBS
0,25% Triton X	250 µl triton-x 100 ml PBS
1% Bovine albumin fraction V solution	25 ml tween 20 solution 0,25 g albumin fraction V
5% Bovine albumin fraction V solution	25 ml tween 20 solution 1,25 g albumin fraction V

In Situ zymography

TRIS buffer solution	1,2 g tris hydrochloride 294 mg calcium chloride dehydrate 1,8 g sodium chloride 10 ml triton X-100 200 ml distilled water
EDTA- solution	50 ml distilled water 9,306 g titriplex III
DQ-Gelatine	1mg DQ-gelatine 1ml distilled water

2.1.4 Devices and materials

Arterial Seldinger wire	Vygen, Elouven, France
Autoclave	VX-95, Systec, Wetttenberg, Germany

Cover slips	Engelbrecht, Edermuende, Germany
Cryomicrotome	CM 1950, Leica Microsystems Wetzlar, Germany
Dako-Pen	Dako, Hamburg, Germany
Drapes	Hartmann, Heidelberg, Germany
Embedding supplies	Sakura Finetek, Alphen aan den Rijn, Holland
Falcon tubes	Greiner Bio-One Kremsmuenster, Austria
Fluorescence microscope	DM2000, Leica Microsystems Wetzlar, Germany
Hydrophobic marking pen	DAKO, Glostrup, Denmark
Incidin Liquid	Ecolab, Wien, Austria
Injection needle	Terumo, Leuven, Belgium
Microscope camera	DFC 425C, Leica Microsystems Wetzlar, Germany
Microcentrifuge tubes	Screensen BioScience Salt Lake City, USA
Peripheral venous catheter	B Braun, Melsungen, Germany
Pipettes	Starlab, Hamburg-Rahlstedt, Germany
Pipette tips	Eppendorf Research Hamburg, Germany
Slides	Marienfeld-Superior, Lauda-Koenigshofen, Germany
Small animal ventilator	Foehr Medical Instruments Seeheim, Germany
Sterile compresses	Hartmann, Heidelberg, Germany
Sterile workbench	BSB 4, Gelaire Sydney, Australia
Surgical sutures	Johnson & Johnson, New Brunswick, USA
Surgical microscope	C-W10xA/22, Nikon Tokio, Japan
Surgical Instruments	Aesculap, Tuttlingen Germany
Syringe	B Braun, Melsungen, Germany
Test animal shaver	Aesculap, Tuttlingen, Germany
Ultrasound machine	HD 11XE, Philips Amsterdam, Holland
Vaporiser	Draeger, Luebeck, Germany

2.1.5 Software

Excel 2010, Office

GraphPad Prism 5.04

ImageJ 1.46 (open source)

Leica Fotosoftware

Word 2010, Office

Mendeley v1.19.2

Microsoft, Redmond, USA

GraphPad Software, San Diego, California
USA

Wayne Rasband, National Institutes of
Health, USA

Leica, Wetzlar, Germany, Application
Suite V3.7

Microsoft, Redmond, USA

Elsevier, London, Great Britain

2.2 Study design

Male Wistar rats (n=44, 22- donor rats, 22- recipient rats) weighing 200g to 250g were obtained from the local animal care facility of the University Duesseldorf, Germany. All experiments were performed in agreement with national animal welfare act and approved by the state animal care committee – reference number 84-02.04.2012.A391.

After explantation of aortic grafts of donor animals, they were decellularized and coated with FN. Thereafter, coated aortic grafts were implanted into the infrarenal aortas of recipients (Fig.2).

The recipient animals were divided into two experimental groups: DCA group (n=12) received decellularized aortic grafts coated with FN and DCA in concentration 0,75 g/l via drinking water, while the control group (n=10) received only decellularized aortic grafts coated with FN (Fig.3); each group was observed for 2 and 8 weeks, respectively (Tab.1).

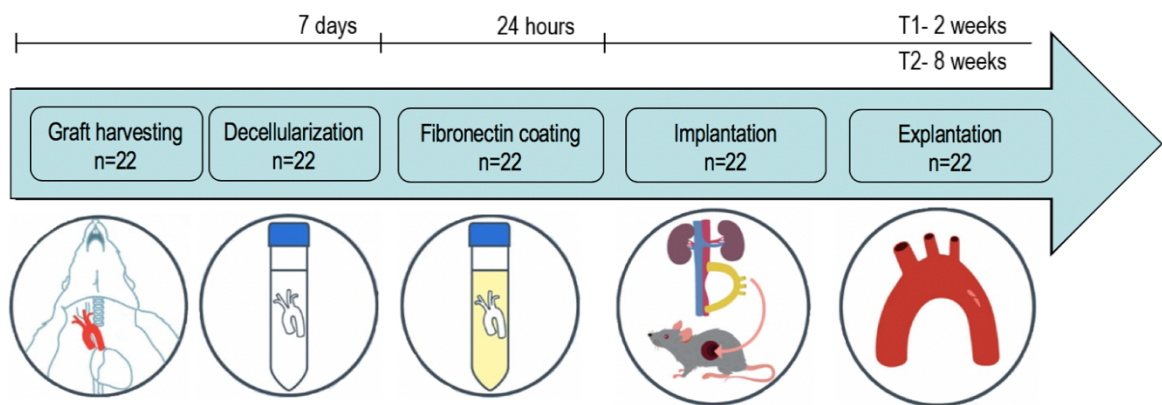


Fig.2: Experimental design: the graft harvesting with next decellularization and surface coating with FN. The preserved aortic grafts were connected in an end-to-side manner with the native aorta of the receiver's animal. Explanation after 2 and 8 weeks.

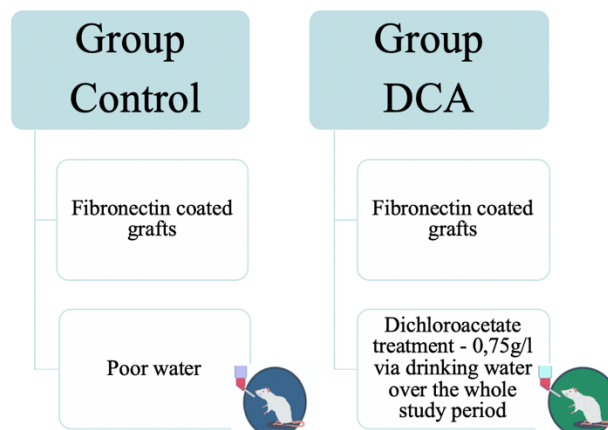


Fig.3: Group design: the recipient animals received FN coated grafts and poor water (Group Control) and DCA in concentration 0,75 g/l via drinking water (Group DCA).

Time	Group Control	Group DCA
2 Weeks	N=5	N=6
8 Weeks	N=5	N=6

Table 1: Overview of the study construction.

2.3 Surgical procedure

2.3.1 Donor operation

Animals were euthanized by an overdose of isoflurane, after which a median sternotomy was performed followed by en bloc removal of the heart and the thoracic aorta. The aortic grafts were prepared containing the ascending aorta, aortic arch, and descending aorta. After thorough preparation, the U-shaped aortic grafts were rinsed with heparinized phosphate buffered saline (PBS).

2.3.2 Decellularization

The decellularization started with four cycles of 12h with 0.5% sodium dodecyl sulfate + 0.5% deoxycholate + 0.05% sodium azide and DNase solution, followed by four repetitive 24 h washing cycles with PBS containing 1% penicillin/streptomycin (Sigma-Aldrich, Taufkirchen, Germany; Invitrogen Carlsbad, USA). All steps were conducted in 15 ml tubes, filled with 12 ml, containing a maximum of two grafts. The solution was changed during the first two days after explantation each 12 h and for the next three days each 24 h. Every time if a new solution was used, the bottle was also changed.

Protokoll:

1. Day 1 – 0 h – Decellularization solution 1
2. Day 1 – 12 h – Decellularization solution 1
3. Day 2 – 22 h – Decellularization solution 2
4. Day 2 – 24 h – Decellularization solution 1
5. Day 3 – 36 h – Decellularization solution 1
6. Day 3 – 46 h – Decellularization solution 2
7. Day 3 – 48 h – Decellularization solution 0
8. Day 4 – 72 h – Decellularization solution 0

9. Day 5 – 96 h – Decellularization solution 0
10. Day 6 – 120 h – Decellularization solution 0
11. Day 7 – 144 h – End of decellularization

For the guarantee of a better mixing of the decellularization solution during the whole time the bottles were stored on a rotator with 220 rotations per minute.

2.3.3 Graft coating with fibronectin

After decellularization vascular grafts were coated with FN. All decellularized rat aortic prostheses intended for implantation (n=22) were incubated under the following conditions: FN concentration 50µg/ml in PBS, incubating time 24 h and incubation temperature 37°C. The incubation occurred in 1 ml test tube on a rotator with 220 rotations per minute.

2.3.4 Recipient procedure

Young recipients' rats (n=22) were anaesthetized by brief isofluran-inhalation and with the help of a Seldinger wire and venous catheter tracheal intubiert. The animals were given artificial respiration during the operation with a frequency by 80 breath per minute and a tidal volume of 1.5 ml by machine.

The operation area was shaved and afterwards a central venous jugular vein catheter was inserted and carprofen was injected intraperitoneally. After systemic administration of 300 IU/kg heparin and aortic clamping within this segment 2 incisions were made to create distal and proximal openings for the anastomoses. The anastomoses were made in an end-to-side manner, with a continuous 10-0 suture (Ethicon, Norderstedt, Germany). The left arteria carotis communis and arteria subclavia have been clipped. The truncus brachiocephalicus was first left open to guarantee a de-aeration, then this departure also has been clipped.

Following release of blood flow through the graft, the native aorta between the two anastomoses was ligated to improve perfusion of the implant. After clinical observation particularly paying attention to the perfusion of the lower extremities, the abdomen was closed and after sonographic confirmation of unimpaired conduit perfusion with a Philips HDX 11 ultrasonography system equipped with a 15 MHz probe the recipients were allowed to recover from anesthesia.

2.3.5 Graft explantation

Two and eight weeks after implantation, recipient rats were anesthetized, and Doppler sonography was conducted to control the perfusion of the prostheses. After median laparotomy in all rats, the aortic grafts were excised, rinsed first with solution (12.5 IE/ml Heparin in PBS). The U-shaped grafts were separated from the receiver's fabric and were frozen for the other histologic processing in embedding supplies in -20°C. The histology preparations were cut and embedded separately.

2.4 Histology

Each of explanted grafts was divided into four regions: proximal anastomosis (A1), ascending aorta (A2), descending aorta (B1) and distal anastomosis (B2). In each region of the graft, 10 representative cross-sections (5 μ m thick) were generated for histological staining (Fig.4).

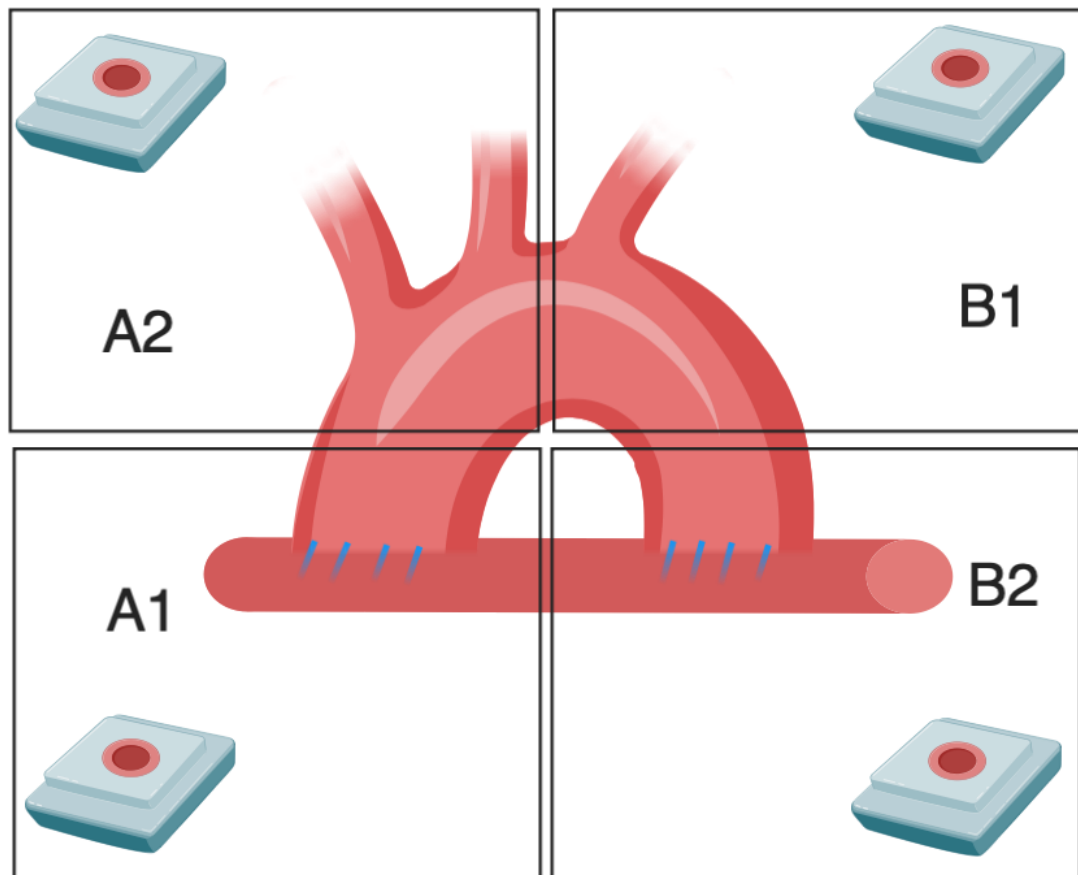


Fig. 4: The schematic drawing represents A1, A2, B1, B2 regions of explanted grafts. Figure is created with BioRender.com .

2.4.1 Hematoxylin-eosin stain

For characterization of the vascular wall and cell layers hematoxylin-eosin (HE) staining was used. The blue coloring hemalum colors nuclei of cells blue. Materials colored blue by hemalum are often said to be basophilic. The eosin colors eosinophilic other structures in various shades of red, pink and orange.

Protocol:

1. Immerse sections in the filtered hematoxylin, 1 min
2. Rinse with distilled water, 1 min
3. Immerse sections in the 4-5% acetic acid, 1 min
4. Rinse with distilled water, 1 min
5. Rinse in cool running water, 2x1 min
6. Dehydrate in 70% alcohol, 1 min
7. Stain with eosin B, 12 min
8. Dehydrate in 70% alcohol, 1 min
9. Dehydrate in 96% alcohol, 2x1 min
10. Dehydrate in 100% alcohol, 2x1 min
11. Clear with 100% xylol, 2x1 min
12. Allow dry
13. Mount coverslip onto the section on glass slide with roti-histokitt

To be able to discover possible histologic differences in the different regions and subregions of the grafts, different subregions were examined separately. Three 5 μ -thickens representative cryosections were made in 2 and 8 post-surgical weeks from each subregion and stained with HE-stain.

2.4.2 Von Kossa stain

The von Kossa stain is intended for use in the histological visualization of calcium deposits. Tissues were treated with a silver nitrate solution combined with the phosphate and the silver was deposited by replacing the calcium reduced by the strong light, and so could be visualized as deep brown. One 5 μ -thickens representative cryosection were made in 2 and 8 post-surgical weeks from each subregion and stained with VK-stain.

Protocol:

1. Aceton fixation in - 20°C, 10 min
2. Allow dry

3. Include positive control (calcific aorta)
4. Rinse with distilled water, 1min
5. Immerse sections in 5% silver solution, place in front of a 60-watt lamp, 1 hour
6. Rinse with distilled water, 3x3min
7. Treat with 2% sodium formaldehyde, 2 min
8. Rinse in running tap water, 10 min
9. Treat with 5% sodium thiosulfate solution, 5 min
10. Rinse in running tap water, 15 min
11. Rinse with distilled water, 3x3min
12. Treat with kernechtrot-aluminum sulfate, 10 min
13. Rinse with distilled water, 3x3min
14. Dehydrate in 70% alcohol, 1x2 min
15. Dehydrate in 96% alcohol, 1x2 min
16. Dehydrate in 100% alcohol, 1x2 min
17. Dehydrate in 100% xylol, 2x5 min
18. Mount coverslip onto the section on glass slide with roti-histokitt

2.4.3 Movat pentachrome stain

Movat-Pentachrome staining was chosen for detection of matrix components. Nucleuses and elastic fibers were colored in purple-black, ground substance and mucin in blue, collagen fibers in yellow, glycosaminoglycans in green, muscle fibers in red and fibrin in bright red. One 5 μ -thickens representative cryosection was made in 2 and 8 post-surgical weeks from each subregion and stained with movat-pentachrome stain.

Protocol:

1. Formaldehyde fixation, 5 min
2. Rinse with distilled water, 5min
3. Treat with 50° Bouin's solution, 10 min
4. Rinse in running tap water, 10 min
5. Treat with 5% sodium thiosulfate solution, 5 min
6. Rinse with distilled water, 2x2min, 1x1min
7. Treat with 1% alcian blue solution, 20 min
8. Rinse in running tap water, 3x3 min
9. Treat with heated alkaline alcohol, 10 min.
10. Rinse in running tap water, 3x3 min

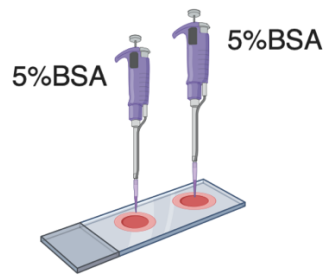
11. Treat with Weigert's iron hematoxylin, 9min
12. Rinse in running tap water, 1 min
13. Rinse with distilled water, 2x2min, 1x1min
14. Treat with brilliant crocein R, 1 min.
15. Rinse with distilled water, 2x2min, 1x1min
16. Treat with 5% phosphotungstic acid solution, 5 min
17. Treat with 1% glacial acetic acid, 5 min
18. Rinse with distilled water, 2x2min, 1x1min
19. Dehydrate in 96% alkohol, 2x1 min
20. Dehydrate in 100% alkohol, 2x1 min
21. Alcoholic safran solution, 8 min
22. Dehydrate in 100% alkohol, 1 min
23. Clear with 100% xylol, 3x5 min
24. Mount coverslip onto the section on glass slide with roti-histokitt

2.4.4 Immunofluorescence stain

Cryo-sections were incubated for 10 min with 4% formalin, for 10 min with 0,25% Triton-X-100 and for 1h with 5% BSA at room temperature. Immunofluorescence staining protocol was applied with primary antibodies: rabbit CD3 (1:200), mouse CD-68-(1:200), mouse anti α SMA-(1:200) and rabbit anti vWF (1:200) for 1h at 37°C. Thereafter the sections were washed three times in PBS containing 0.1% Tween-20. Secondary antibodies Alexa 546 (anti-mouse, 1:300) and Alexa 488 (anti-rabbit, 1:300) + 1% BSA were applied for 45 min at 37°C. Control sections were incubated without primary antibodies with PBS. After 1h incubation, sections were again washed three times in PBS. Sections were covered with vetaschild antifade mounting medium with DAPI and the cover slips were fixed with the help of nail polish. Image acquisition was performed with a microscope system DM 2000, equipped with a digital Application Suite V3.7 software.

Protocol:

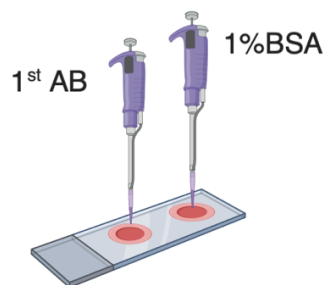
1. Formaldehyde fixation, 10 min
2. Rinse with PBS, 3x1min
3. Treat with 0,25% triton X-100, 10 min
4. Rinse with PBS, 3x1min
5. Blocking solution 5% BSA in PBS at room temperature, 1 h



Created with BioRender.com

6. Treat with 0,1% tween, 3x1min

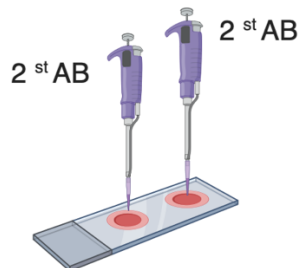
7. Incubate with the 1st antibody in the blocking solution at 37°C (light protected), 1 h



Created with BioRender.com

8. Treat with 0,1% tween, 3x5min

9. Incubate with 2nd antibody min at 37°C (light protected), 45 min



Created with BioRender.com

10. Rinse with PBS, 3x5min

11. Mount the cover slips with dapi mounting medium

12. Seal the cover slips with polish nail.

Smooth muscle cells were visualized with the anti α -SMA (1:200, mouse), endothelial using anti-vWF (1:200, rabbit). Neutrophils were detected with rabbit CD3 and macrophages with mouse CD-68 antibodies.

2.4.5 *In Situ* zymography

In Situ-zymography is a procedure which allows to show the activity of the matrix-metalloprotease (MMP). Five-micrometer-thick sections were incubated with 40 μ g/ml

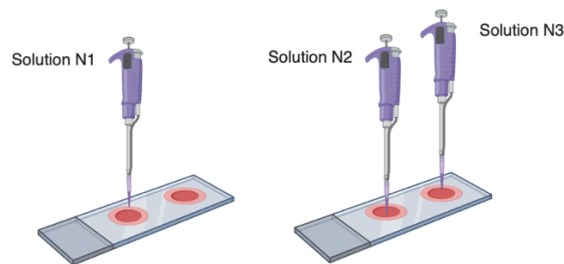
fluorescein-conjugated gelatin in 50 mmol/l Tris-HCl, 10 mmol/l CaCl₂, 150 mmol/l NaCl, 5% Triton-x-100 for 24 h at 37°C. Sections were washed 5 times with PBS and distilled water and mounted with vetashield antifade mounting medium with DAPI.

Protocol:

1. Prepare solutions

<u>N1 - Working solution</u>	<u>N2 - Negative Control 1</u>	<u>N3 - Negative control 2</u>
2 µl DQ-Gelatine	2 µl EDTA- solution	200 µl TRIS buffer solution
198 µl TRIS buffer solution	2 µl DQ-Gelatine	
	196 µl TRIS buffer solution	

2. Incubate with solutions at 37°C, 20 h



Created with BioRender.com

3. Rinse with PBS, 3x2min

4. Mount the cover slips with vectashield antifade mounting medium with Dapi

5. Seal the cover slips with polish nail

Comparative quantification of the MMP activity was performed with Image J by measuring the mean fluorescence intensity of the aortic graft wall.

2.5 Morphological characterization of explanted grafts

2.5.1 Neointima formation

In each vascular graft in each subregion (A1, A2, B1, B2) three HE-stained cross-sections were undergoing neointima quantification. Comparative quantification of luminal neointima formation was performed by standardized scoring. HE-stained cross-sections were divided into the eight segments (Fig. 5a) in which the luminal endothelialization was quantified and the media thickness and the thickness of the neointima were measured to determine an intima-to-media ratio (Fig. 6).

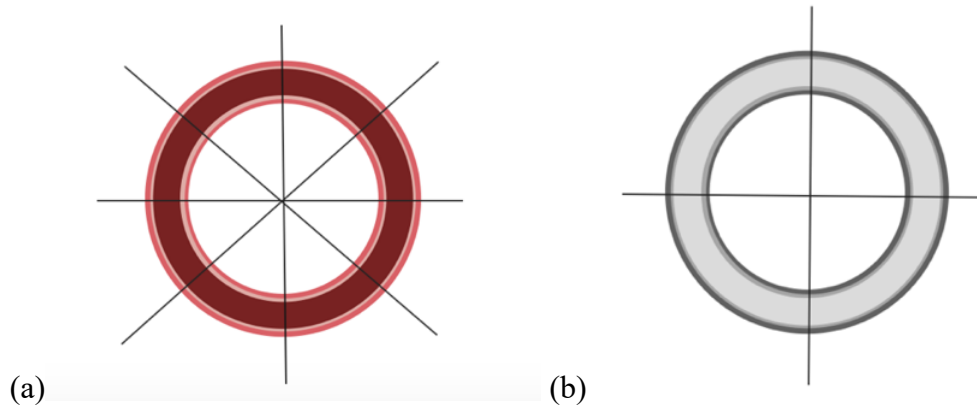


Fig.5: The schematic drawing represents cross-sections through each region of the conduit and display the subdivision into eight (a) and four (b) pieces.

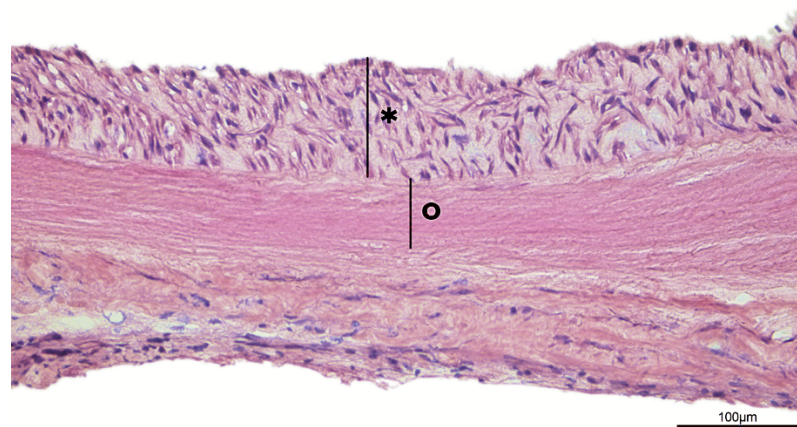


Fig.6: Intima-to-media measurement in hematoxylin eosin stain; (asterisk-neointima, circle-media). Scale bars 100µm. Magnification 20x.

$$\text{Intima Media Ratio} = \frac{\text{Thickness of intima}}{\text{Thickness of media}}$$

2.5.2 Media repopulation

The total number of cells invading the medial part of the decellularized implants was counted out under the light microscope in the whole cross section. By analogy with neointima quantification slides were examined in all 4 subregions of the grafts.

2.5.3 Calcification

In each region, one cross section was stained with VK stain. The stained sections were divided into four segments (Fig. 5b), where calcification level was calculated in intima and media using the calcification score (Table 2), and finally, the mean value was determined.

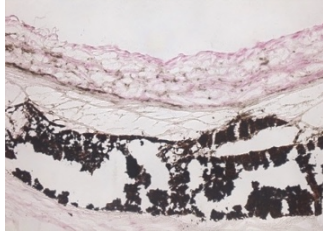
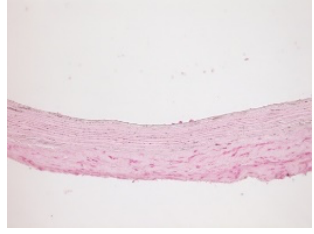
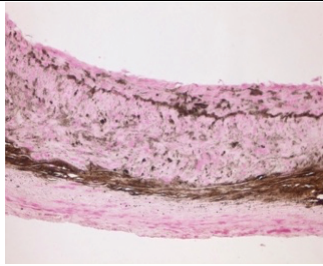
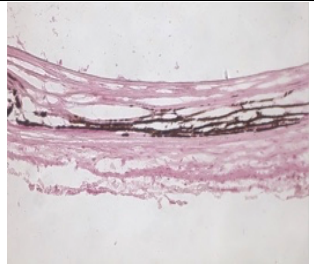
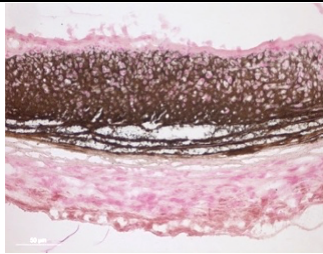
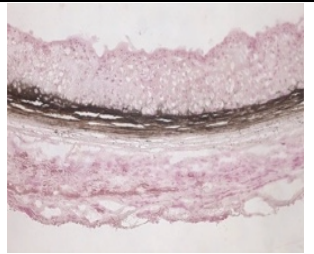

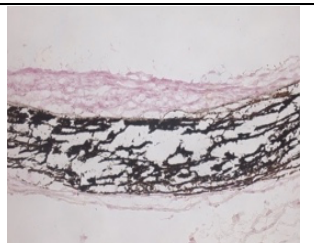
Intima		Media	
1=microcalcification		1=microcalcification	
2=macrocalcification <50% of the neointima area		2=macrocalcification <25% of the area	
3=macrocalcification >50% of the neointima area		3=macrocalcification 25-50% of the area	
		4=macrocalcification 50-75% of the area	
		5=macrocalcification >75% of the area	

Table 2: Intima and media calcification score table (Assmann *et al.*, 2014).

2.5.4 MMP Activity

In situ zymography revealed remarkable matrix MMP activity around the media-repopulating cells as well as in the neointima. Standardized photos of the green canal (488 nm) were taken up for the evaluation with the picture processing software ImageJ. The middle grey step without unity (Mean Gray Value) enables to make a declaration about the fluorescence intensity. With the regulation of the grey step the value 0 and the color white the maximum point value is assigned to the color black. The middle grey step corresponds to the sum of all grey values in the decisive area partly by the number of the pixels. Because only one color canal was taken up, a conversion is not necessary in an uncolored black grey-white semitone picture. With all pictures the area to be valued (region of interest = ROI) was determined by hand and the middle grey step was calculated.

2.5.5 Statistical analysis

Data are presented as mean values \pm SEM for all continuous variables. An unpaired t-test was used to compare the means of the two groups, and two-way analysis of variance (ANOVA) analyses were used to compare the differences between the time-points. Statistical significance was considered if p-values were lower than 0,05. Data analysis was conducted using the Graph Pad Prism v5.04 (Graph Pad Software, San Diego, USA).

2.6 ETHICS VOTE AND ANIMAL EXPERIMENT APPROVAL

All experiments were performed in agreement with the national animal welfare act and approved by the state animal care committee – reference number 84-02.04.2012.A391.

3. Results

3.1 Operative results

All 22 decellularized aortic grafts, coated with FN, were successfully implanted and remained functional for up to 2 and 8 weeks, after which they were explanted. All animals showed normal clinical function and recovered without signs of neurological or ischemic symptoms of the lower limbs.

3.2 Neointima and media formation

Histologic assessment showed that neointima formation was observed in all explanted grafts (Tab.3). 2 weeks after transplantation grafts were partially covered with neointima. While after 8 weeks, the luminal surface underwent fast cellular repopulation and recellularized area amounted to 100% (Fig. 7).

The luminal recellularization, determined as the percentage of the luminal neointima formation, increased significantly from week 2 to week 8 ($p < 0.001$), however without statistical intergroup difference.

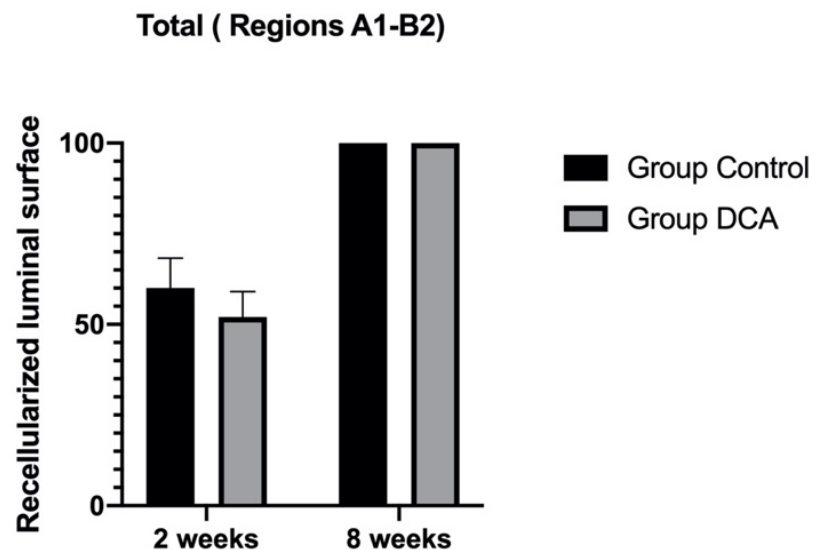




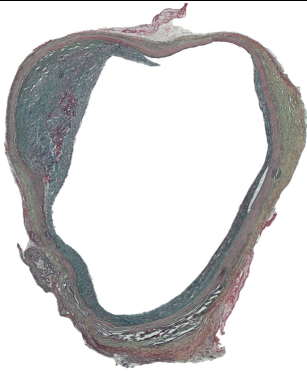



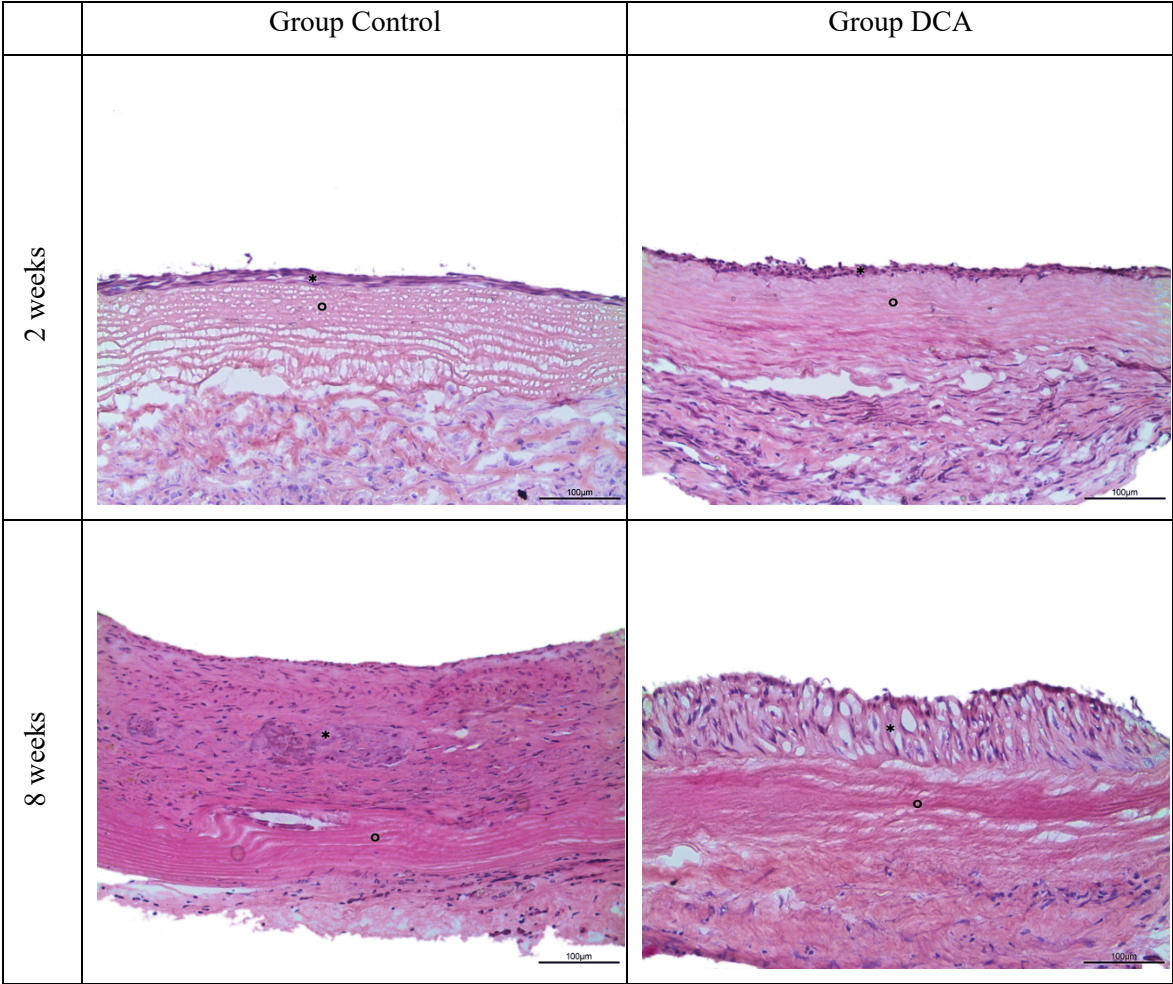


Fig.7: Semiquantitative analysis of luminal recellularization of conduit explants at 2 and 8 weeks.

	Movat pentachrome stain	Von Kossa stain
2 weeks Group Control		
2 weeks Group DCA		
8 weeks Group Control		
8 weeks Group DCA		

Tab.3: Representative images of Movat's pentachrome and von Kossa staining of explanted AGs in control and DCA groups after 2 and 8 weeks *in vivo*. Scale bars = 50 μ m. Magnification 5x.

Neo-intima was mainly presenting as a single-cell layer after 2 weeks. After 8 weeks, luminal surface was presented with multi-layer neointima. Hematoxylin and eosin staining revealed a major increase in cell layers during 8 weeks in control group and a slower increase in group DCA (Tab.4).



Tab.4: Luminal graft recellularization after 2 and 8 weeks *in vivo* (asterisks-neointima, circles-media). Representative images of hematoxylin and eosin (H&E). Scale bars 100 µm. Magnification 20x.

In order to examine neointima, the neointima-to-media ratio was calculated. After 2 weeks on the level of the distal anastomosis (region B2), the intima-to-media ratio in group DCA was significantly decreased as compared to group C (0.7963 ± 0.1518 vs 2.368 ± 0.7953 , $p < 0.05$).

After 8 weeks, in three of the four regions of the implants in DCA group the intima-to-media ratio was significantly lower than in C group (region A1: 1.73 ± 0.24 vs 1.095 ± 0.13 , $p < 0.05$; region A2: 2.79 ± 0.72 vs 0.85 ± 0.1 , $p < 0.05$; region B1: 2.41 ± 0.5 vs 0.98 ± 0.1 ,

$p<0.05$; region B2: 0.95 ± 0.21 vs. 0.54 ± 0.07 , n.s.) (Fig.8 B,C,D,E). In comparison to 2 weeks, there was no significant difference after 8 weeks in distal anastomosis (B2) region.

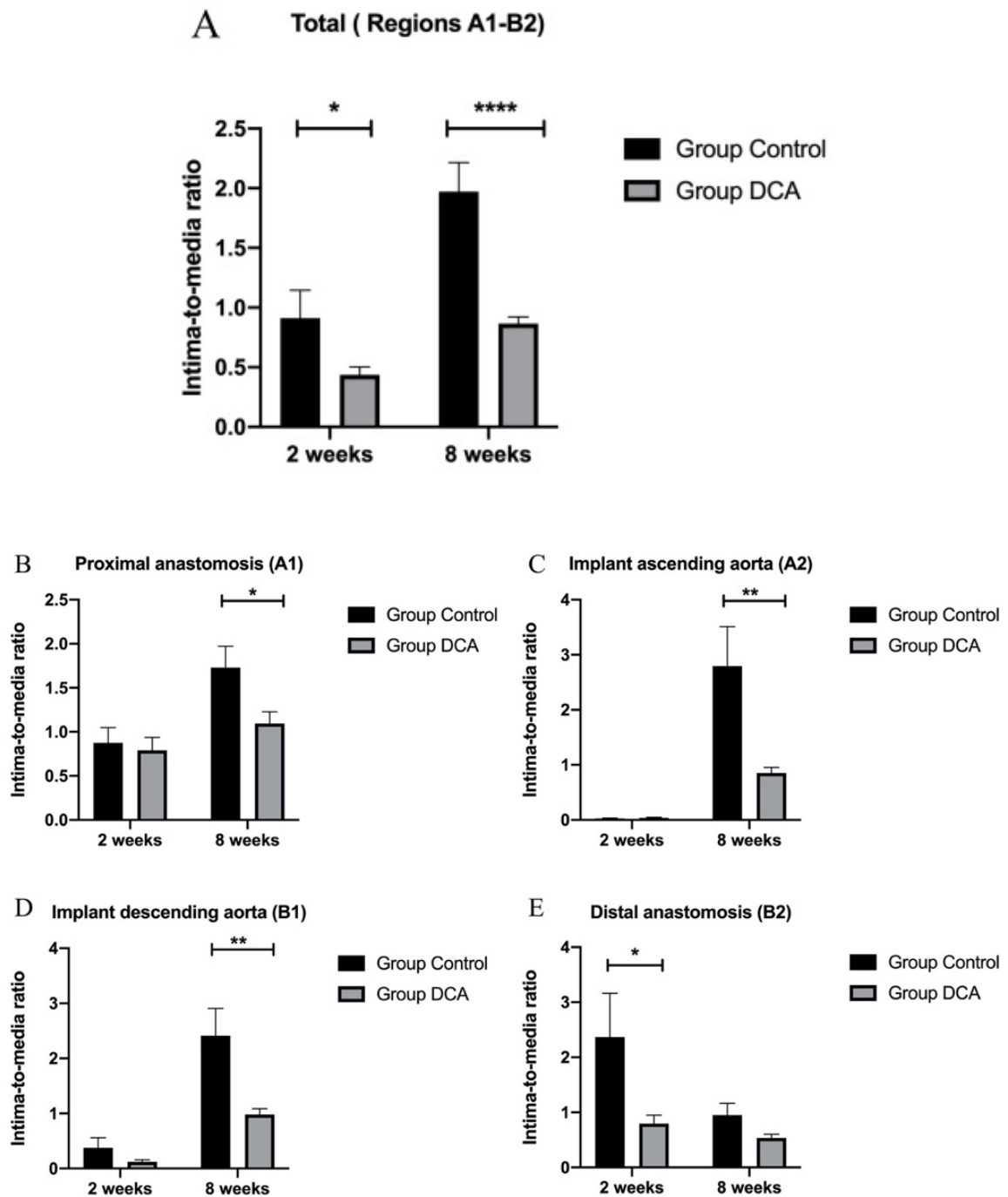
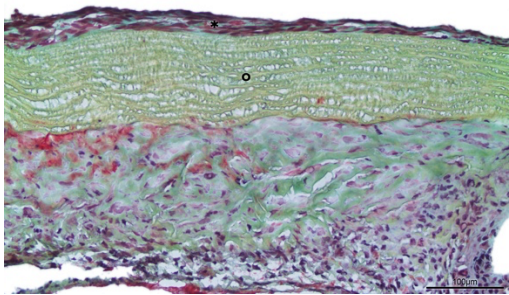
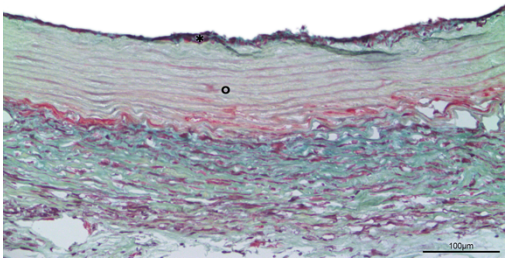
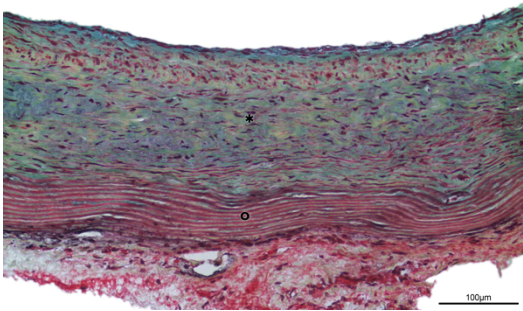
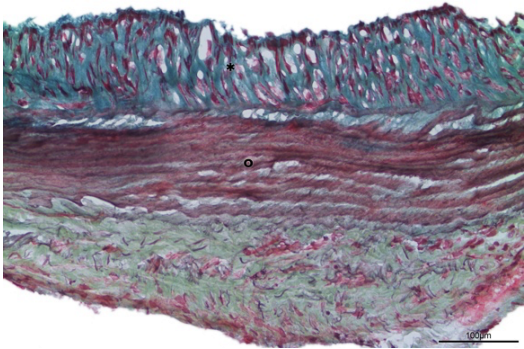


Fig.8: Semiquantitative analysis of the intima-to-media ratio total (A) and in each of the regions (B,C,D,E) of the aortic graft explants in DCA and control groups after 2 and 8 weeks *in vivo*. Mean \pm SD, $p<0.05$; $p^{}<0.01$ $p^{****}<0.001$.**

During the study the overall functional endothelium formation was significantly decreased in the DCA group (0.87 ± 0.06 vs. 1.97 ± 0.24 ; $p<0.001$) (Fig. 8A).

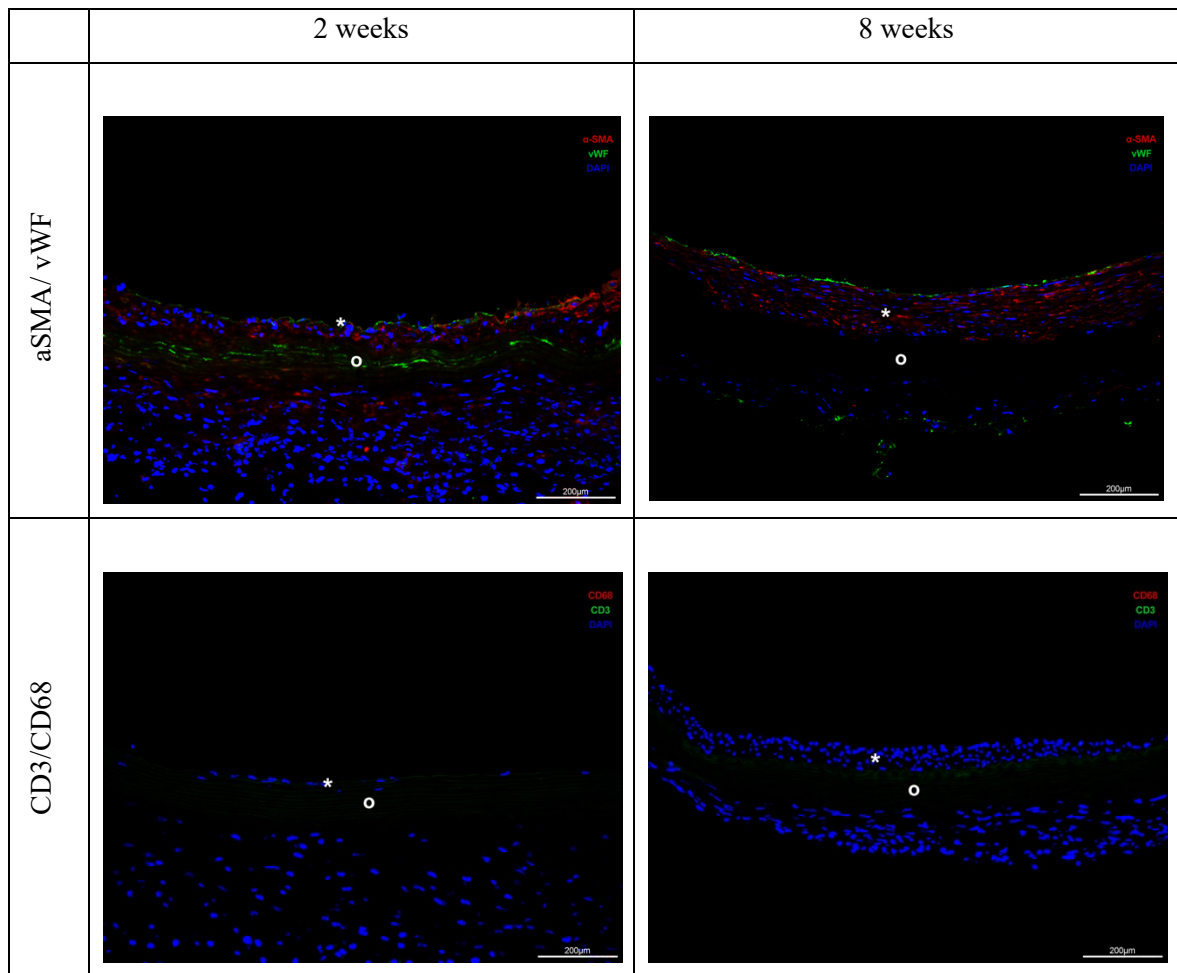
In all grafts, the structure of the neointima was well maintained as visualized by the Movats pentachrome stain with typical yellow staining indicating collagen and blue staining indicating glycosaminoglycans (Tab.5).

	Group Control	Group DCA
2 weeks		
8 weeks		

Tab.5: Representative images of Movat pentachrome stain (asterisks-neointima, circles-media) Scale bars 100 µm. Magnification 20x.

To analyze the cell populations participating in the development of neointima of vessel grafts, sections were stained for SMC marker aSMA, endothelial cells marker vWF, inflammatory cell markers CD3 (for T cells) and CD 68 (for macrophages).

Immunofluorescence staining disclosed vWF positive monolayer indicating an endothelial lining at the luminal surface, identifying them as newly formed endothelium, and multilayered regions stained positive for aSMA (Tab.6).



Tab.6: Representative images of aSMA/vWF and CD3/ CD68-stained explanted aortic grafts in DCA group after 2 and 8 weeks *in vivo* (asterisks-neointima, circles-media).

aSMA/vWF stainig: single-cell layer on the luminal surface stained positive von Willebrand factor (green), multilayered hyperplastic regions stained positive for a-smooth muscle actin (red).

CD3/CD63 staining showed complete absence of immune cells within recellularized grafts. Scale bars = 200 µm. Magnification 10x.

Staining against the inflammatory cell markers CD3 and CD68 was negative throughout all groups (Tab.6).

After 2 weeks, the adventitial surface of explanted aortic grafts was covered with recipient cells, and autologous cell migration into the media was shown after 2 and 8 weeks in both groups (Tab.7). Implant areas close to the anastomoses were re-endothelialized earlier than regions remote to the anastomotic sites. The absolute count of cells repopulating the media did not differ between the groups after 2 and 8 weeks (Fig.9).

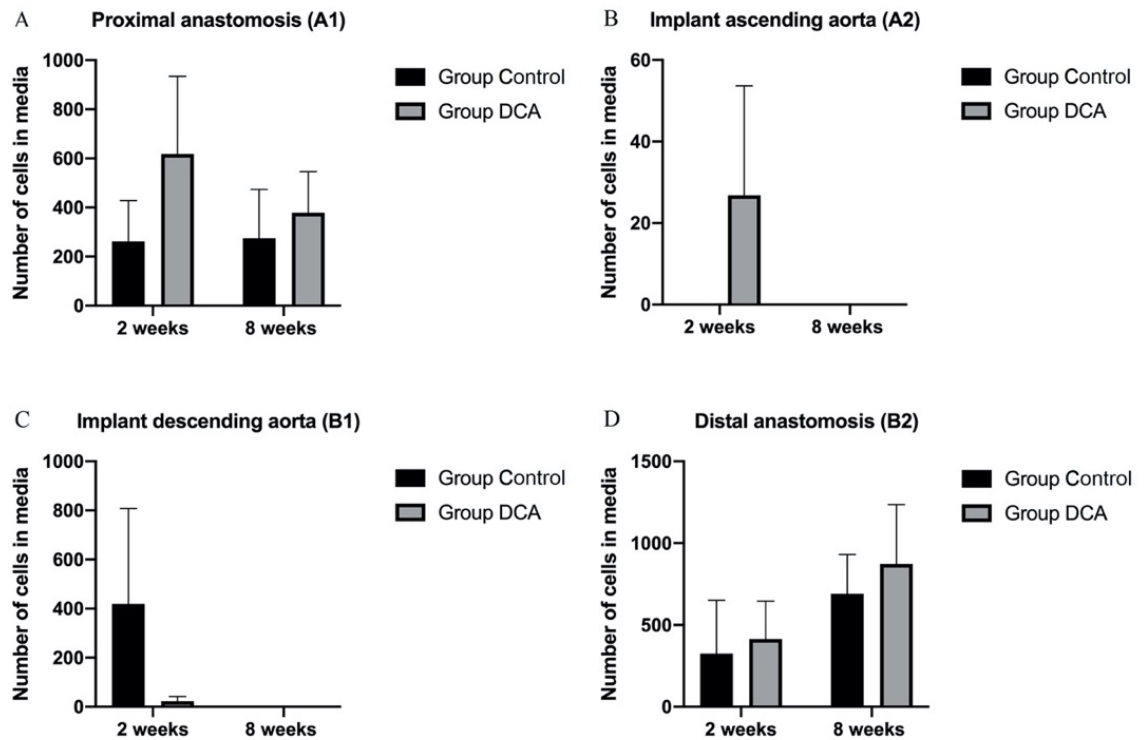
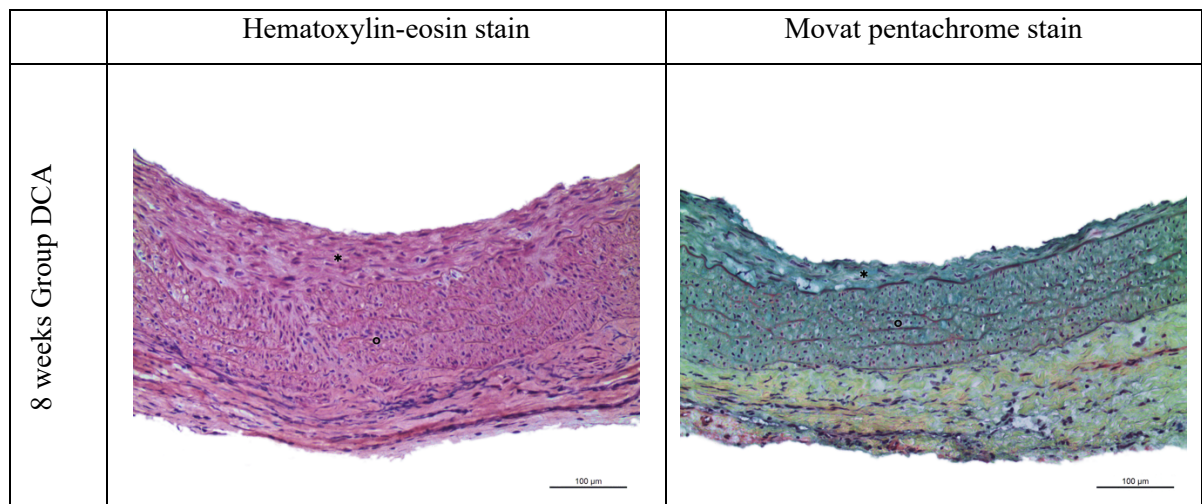
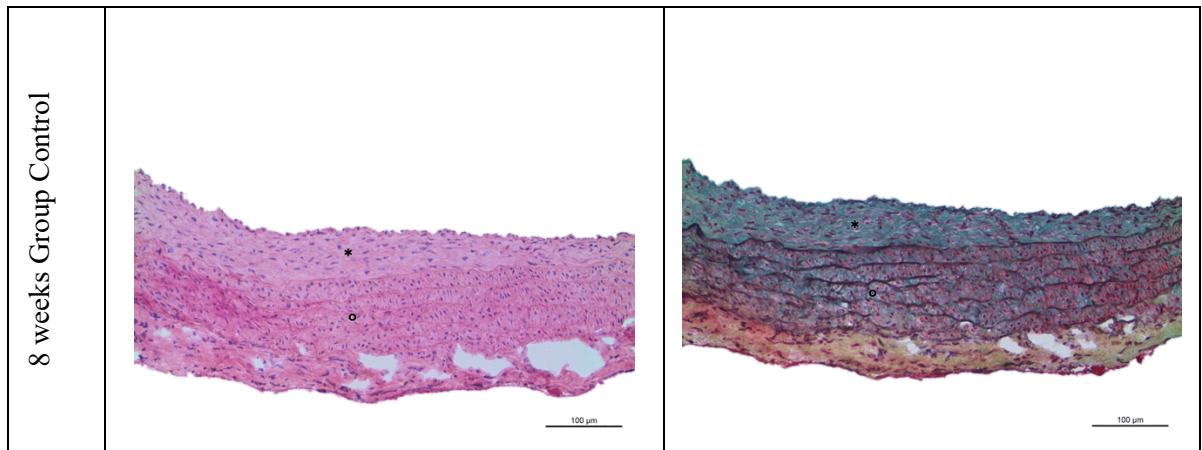


Fig. 9: Semiquantitative analysis of the media re-endothelialization in different regions of the aortic graft explants in DCA and control groups after 2 and 8 weeks *in vivo*.

Cells that infiltrated media were positive for aSMA, whereas inflammatory cell markers were not detected at any time point.

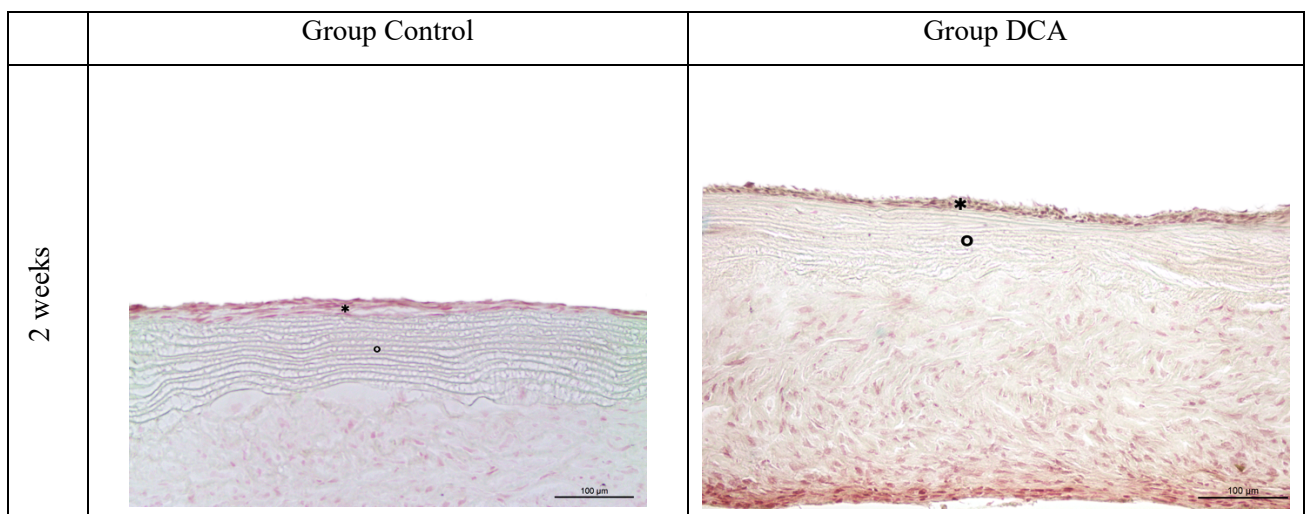


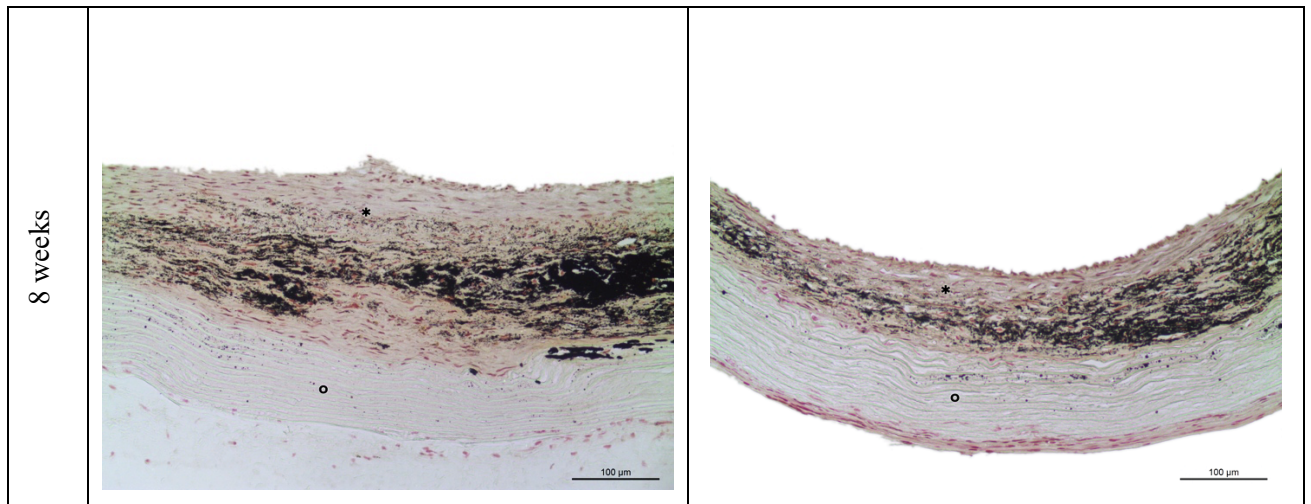


Tab.7: Representative images of repopulation of the aortic graft media in Control and DCA groups after 8 weeks *in vivo* (asterisks–neointima, circles–media). Hematoxylin/eosin and Movat pentachrome stainings. Scale bars = 100 µm. Magnification 20x.

3.3 Neointima and media calcification

Calcification in the explanted grafts was visualized by VK hydroxyapatite staining. VK staining of aortic cross-sections revealed extensive hydroxyapatite deposition predominantly in the aortic neointima and media of animals in group C after 8 weeks, whereas in group DCA, it resulted in slowly progressing media micro-calcification (Tab.8).





Tab.8: Representative images of von Kossa stain in control and DCA groups after 2 and 8 weeks *in vivo*. Scale bars 100 µm. Magnification 20x.

A semiquantitative determination of the calcium content was performed by applying a scoring system based on VK staining. The calcium burden in the neointima after 8 weeks of the DCA group grafts was significantly lower than in control group (region A1: 0.2083 ± 0.1039 vs. 0.8500 ± 0.2927 , $p < 0.05$; region A2: 0.0416 ± 0.0416 vs. 0.8000 ± 0.2865 , $p < 0.01$; region B1: 0.4167 ± 0.1694 vs. 1.200 ± 0.2575 , $p < 0.05$; region B2: 0.2083 ± 0.1343 vs. 0.8000 ± 0.2128 , $p < 0.05$) (Fig. 10).

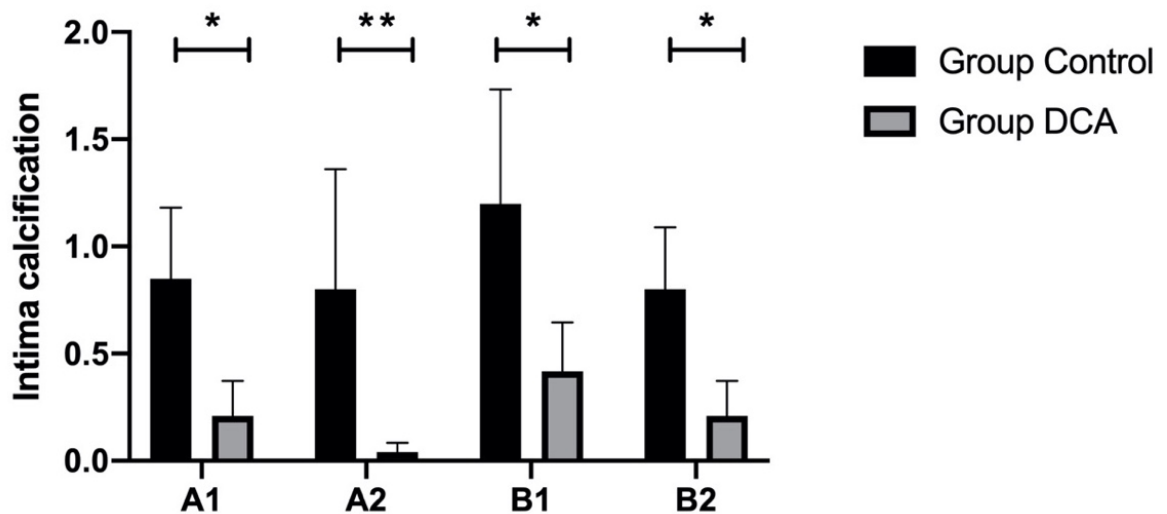


Fig.10: Semiquantitative analysis of the intima calcification in different regions of the conduit explants. DCA significantly inhibited intima calcification of implanted grafts in experimental group after 8 weeks *in vivo*. Mean \pm SD, $p < 0.05$; $p < 0.01$.

The calcium content in media at 2 and 8 weeks show a significant difference only in region A1 in group DCA after 8 weeks (Fig. 11).

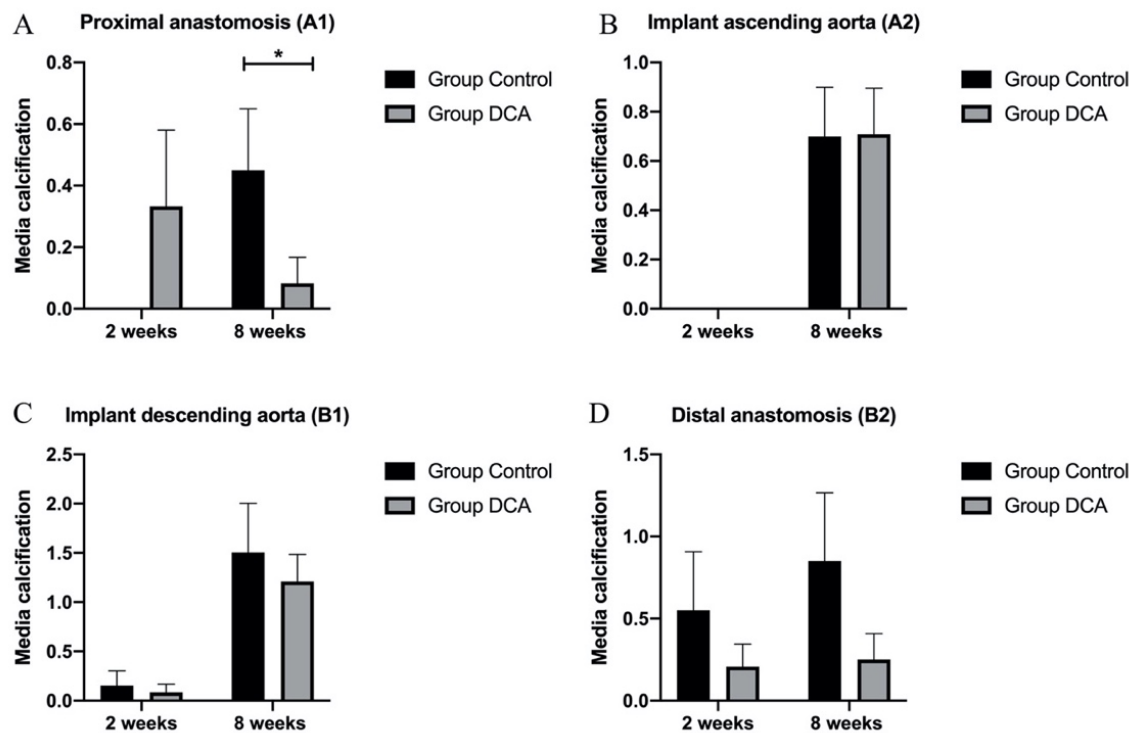


Fig.11: Semiquantitative analysis of the media calcification in different regions of the conduit explants at 2 and 8 weeks. Mean \pm SD, $p^* < 0.05$.

3.4 In situ zymography

In order to examine the MMP activity, in situ zymography was conducted. Staining revealed remarkable MMP activity around the media-repopulating cells as well as in the neointima. 2 and 8 weeks after implantation, the MMP activities of both groups did not differ (Fig. 12).

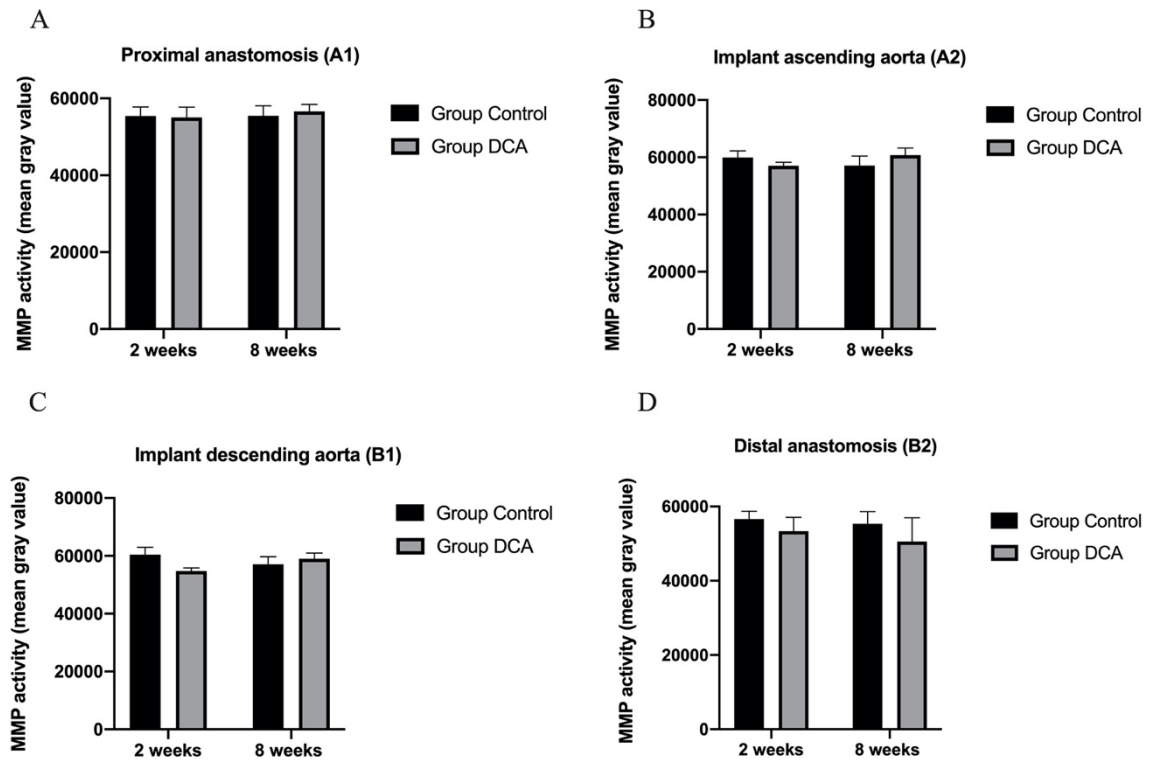


Fig.12: Semiquantitative analysis of MMP activity in each of regions of the conduit explants at 2 and 8 weeks in control and DCA groups.

4. Discussion

The first report on anastomotic intima thickening was noted during the first decade of the 20th century and has been attributed to Carrel and Guthrie: “*within a few days after operation, the stitches placed in making the anastomosis became covered with a glistening substance similar in appearance to the normal*” (Lemson *et al.*, 2000). Two types of vascular remodeling are distinguished: 1) classical remodeling involving medial smooth muscle hyperplasia and increased adventitia volume, and 2) intimal hyperplasia (Mills, Robb and Larson, 2012).

Intimal hyperplasia is the thickening of the tunica intima of a blood vessel as a complication of a reconstruction procedure or endarterectomy. It involves all vessel components, including fibroblast activation, ECM remodeling, and, most notably, endothelial cell-mediated VSMC differentiation, proliferation, and migration, provoked by injury, inflammation, and stretching. Intimal hyperplasia is an important reason for late bypass graft failure, particularly in vein and synthetic vascular grafts.

Different scientific groups have studied processes potentially leading to vascular implant-associated IH. Three conditions are assessed and reported in the literature:

- I. A low wall shear stress
- II. A high solid mechanical stress
- III. A mismatch between compliance and geometry (Felden, Ku and Chaikof, 2005).

The need for biocompatible vascular prostheses led to the development of TEVGs. Although many improvements have been achieved in the recent past, an ideal vascular prosthesis has not been developed until now (Carrabba and Madeddu, 2018). Acellular and decellularized TEVGs ensure minimal immunogenicity but are simultaneously prone to causing thrombosis due to the absence of an endothelial lining. Numerous bioactive surface coatings have been explored to accelerate the autologous *in vivo* recellularization and improve antithrombogenic properties to overcome these limitations. It was shown that a FN coating is biocompatible but accelerated medial graft repopulation and neointima formation, leading to IH (Assmann *et al.*, 2013). Different drugs have been evaluated for their inhibition of IH (Collins *et al.*, 2012). Most of them showed no effect; however, a few indicated potentially favorable outcomes.

As mentioned in the literature review, IH development is associated with a high proliferation rate and resistance to apoptosis. PDK2 is a regulatory key enzyme for mitochondrial metabolism (Dong Wang, 2015), and we suggested that target mitochondrial

therapy may prevent IH and vessel restenosis. As a mitochondrial PDK2 inhibitor, DCA prevents mitochondrial membrane potential hyperpolarization and facilitates apoptosis (Deuse *et al.*, 2014). Based on this statement, we examined the impact of DCA on the development of IH and degeneration of FN-coated decellularized aortic grafts and answered the following questions:

1. Does DCA treatment influence graft recellularization?
2. Does systemic DCA treatment prevent IH?
3. Does systemic DCA treatment prevent graft calcification?

Dichloroacetate is a by-product of drinking water chlorination and a metabolite in the biotransformation of several pharmaceuticals (Stacpoole *et al.*, 1998). The use of DCA began in 1973. It has been researched regarding the treatment of severe metabolic disorders, including diabetes and hypercholesterolemia, lactic acidosis, and cancer (Michelakis, Webster and Mackey, 2008). Since 1987, DCA has been used in scientific studies on treating the effects of brain ischemia (Marangos *et al.*, 1999). In 2007, it was discovered that DCA produced a positive response with implanted tumors of the lung and brain and human breast cancer. Since 2009, it has been used as an alternative therapy for treating cancer in the first DCA clinics (Khan, Andrews and Blackburn, 2016). DCA is a selective drug and, unlike cytotoxic chemotherapy drugs, it does not poison healthy tissues. DCA inhibits mitochondrial PDK, which is formed in high concentrations in tumor cells, and thus the breakdown of pyruvate. However, pyruvate is essential for healthy cell metabolism and the function of the respiratory chain, including glucose oxidation. Increased pyruvate breakdown by PDK shifts the metabolic pathway from effective aerobic adenosintriphosphat (ATP) production to ineffective anaerobic glycolysis in the mitochondria. DCA induces apoptosis and inhibits cell proliferation and tumor growth with no discernible toxicity (Deuse *et al.*, 2014).

Most people who take DCA tolerate it well. Others show mild side effects, including fatigue, confusion, memory loss, sedation, tremors, hallucination, agitation, and depression. Side effects could be mitigated by dietary supplements or a break from the treatment (Mills, Robb and Larson, 2012). Simultaneously, Peter Stacpoole demonstrated that therapeutic use of sodium DCA caused no and mild side effects, and the probability of developing side effects depended on the dose and age of the patient (Stacpoole, Gilbert, *et al.*, 2008). A small contingent of the population metabolizes DCA slowly and reducing the dose should solve this issue.

The most common dose-dependent side effect associated with DCA therapy is reversible peripheral neuropathy (Stacpoole, Kurtza, *et al.*, 2008). This is particularly common in patients with mitochondrial encephalomyopathy, lactic acidosis, and stroke-like episodes (MELAS) receiving oral doses daily for a prolonged time (Anselm and Darras, 2006). Peripheral neuropathy often complicates MELAS because these patients also have predisposing factors such as diabetes and diabetes-associated peripheral neuropathy (Michelakis, Webster and Mackey, 2008). Our experiments were performed with 0.75 g/L DCA *via* drinking water because DCA has been used safely at this dose and does not cause side effects (James and Stacpoole, 2016).

4.1 Influence of dichloroacetate on graft recellularization

The importance of a functional endothelium in preventing thrombosis is well documented in the literature. When collagen of the vessel wall is exposed, usually by damage to the endothelium, platelets bind directly to the vessel wall and eventually initiate coagulation. Surface coating decellularized vascular grafts with FN, laminin, SDF1 α , fibrin, or vascular endothelial growth factor has been shown to accelerate the *in vivo* adhesion of recipient cells (Toshmatova *et al.*, 2019) (Sugimura *et al.*, 2020).

Since DCA induces apoptosis, it was important that it did not interfere with reendothelialization of vascular grafts. In our study, anastomotic regions showed recellularization earlier than non-anastomotic regions. This finding proves the theory that neointima formation on cardiovascular implants chiefly occurs from the anastomotic regions (Chan *et al.*, 2017). We also found neointima distant from the anastomoses after 2 weeks. Histological assessment showed neointima formation in all explanted grafts: after 2 weeks, they were partially covered with neointima, while after 8 weeks, the luminal surface showed complete fast cellular repopulation. The neointimal areas were populated by α SMA-positive myofibroblasts without staining positive for inflammatory markers.

Thus, DCA does not prevent recellularization of aortic grafts and does not induce an inflammatory reaction.

4.2 Influence of dichloroacetate on intimal hyperplasia

Since the 1970s, IH has been recognized as a cause of restenosis and graft failure (Collins *et al.*, 2012). Intimal hyperplasia may result from trauma, vascular surgery, turbulent flow, vasospasm, and ischemia. Aggravated neointima formation is specific to all

forms of vascular grafts, including venous and prosthetic conduits used in coronary and peripheral arterial bypass.

To achieve biocompatibility of the TEVGs, controlling the development of neointimal hyperplasia is essential. Despite the low thrombogenicity of decellularized FN-covered aortic grafts, they are predisposed to aggravated neointima formation. Therefore, in our study, we examined the effects of DCA on intima formation, as previously described.

All explanted aortic grafts were covered with neointima at both time points. A single-cell layer neointima could be observed in vascular grafts after 2 weeks, while after 8 weeks, all grafts presented with multilayer neointima. To determine the presence of IH, we calculated a neointima-to-media ratio, as described previously. After 8 weeks, this ratio was significantly decreased in the DCA group, as was the overall functional endothelium formation.

The histological structure of the functional neointima was well visualized by Movat pentachrome stain, with typical yellow staining indicating collagen and blue staining indicating glycosaminoglycans. Immunofluorescence enabled identification of a newly formed endothelial lining at the luminal surface positively stained for vWF and aSMA with the absence of inflammatory cell markers CD3 and CD68 throughout all groups.

The present study provides evidence that DCA can suppress intimal hyperplasia.

4.3 Influence of dichloroacetate on graft calcification

Current small-diameter commercial vascular grafts are prone to progressive *in vivo* thrombosis, calcification, and infection and have no growth potential. Beyond inhibition of hyperplasia, the present study revealed a significant inhibitory effect of DCA on degenerative calcification in the neointima within only 8 weeks after graft implantation and a tendency toward inhibition of media calcification. As we have previously shown for *in vivo* recellularized grafts, calcification of the neointima in the present experiments occurred predominantly in areas of hyperplastic intima formation. Therefore, the observed hyperplasia reduction by DCA appears causal in the inhibition of implant calcification. According to previous studies on vascular and valvular grafts decellularized with our detergent-based protocol, implantation of the prostheses in the present study did not result in a detectable inflammatory response, indicating effective donor cell removal during the decellularization process (Assmann *et al.*, 2017).

To the best of our knowledge, we revealed for the first time that DCA protects tissue-engineered prostheses from calcification.

4.4 Limitations

In this study, systemic DCA therapy effects on the degeneration of the decellularized vascular grafts in a small animal model were successfully described. While this established rodent model offers a resourceful and time-saving alternative to large animal experiments, not all results can be adopted for human use. This study has several limitations.

First, the rodent model is limited by the anatomy and physiology of the test animals. Rats and mice have a natural resistance to the development of atherosclerosis and differ from humans in genetic expression and cholesterol metabolism, so they are less prone to cardiovascular degeneration than humans (Zhao *et al.*, 2020). Further preclinical studies, preferably in an adequate large animal model, are necessary to examine the effects of DCA on a graft's degeneration.

Second, although the follow-up period of 8 weeks was sufficient to observe a significant difference in the degeneration of the decellularized FN-coated aortic grafts between DCA and the control group, it is a short time to predict long-term results.

4.5 Perspectives

Intimal hyperplasia and restenosis are major issues in cardiac and vascular surgery after bypass operations and in cardiology after angioplasty and endovascular surgery. Despite advances in stent technology such as drug-eluting stents, restenosis continues to be a problem following percutaneous coronary intervention. An orally administered medication might prevent cell proliferation and occlusion of the vessel lumen. Systemic DCA treatment in our study shows reduced neointima formation while allowing rapid reendothelialization of the implants. Future studies in this area could focus on oral DCA administration to determine whether this approach is effective in humans who undergo endovascular or bypass surgery and to evaluate side effects.

5. References

- Akbari Zahmati, A. H. *et al.* (2017) 'Chemical Decellularization Methods and Its Effects on Extracellular Matrix', *Internal Medicine and Medical Investigation Journal*, 2(3), p. 76. doi: 10.24200/imminv.v2i3.63.
- Alexi-Meskishvili, V. *et al.* (2000) 'Optimal conduit size for extracardiac Fontan operation', *European Journal of Cardio-thoracic Surgery*, 18(6), pp. 690–695. doi: 10.1016/S1010-7940(00)00593-5.
- Alizadeh-Osgouei, M., Li, Y. and Wen, C. (2019) 'A comprehensive review of biodegradable synthetic polymer-ceramic composites and their manufacture for biomedical applications', *Bioactive Materials*. Elsevier, 4(1), pp. 22–36. doi: 10.1016/j.bioactmat.2018.11.003.
- Altman, G. H. *et al.* (2003) 'Silk-based biomaterials.', *Biomaterials*. Netherlands, 24(3), pp. 401–416. doi: 10.1016/s0142-9612(02)00353-8.
- America, N. *et al.* (2020) '2020 Heart Disease & Stroke Statistical Update Fact Sheet Congenital Cardiovascular Defects Congenital Cardiovascular Defects - 2020 Statistical Fact Sheet', (Ccd).
- Anselm, I. A. and Darras, B. T. (2006) 'Dichloroacetate causes toxic neuropathy in MELAS: A randomized, controlled clinical trial', *Neurology*, 67(7), pp. 1313 LP – 1313. doi: 10.1212/01.wnl.0000243807.14293.07.
- Assmann, A. *et al.* (2013) 'Acceleration of autologous invivo recellularization of decellularized aortic conduits by fibronectin surface coating', *Biomaterials*. Elsevier Ltd, 34(25), pp. 6015–6026. doi: 10.1016/j.biomaterials.2013.04.037.
- Assmann, A. *et al.* (2014) 'The degeneration of biological cardiovascular prostheses under pro-calcific metabolic conditions in a small animal model', *Biomaterials*, 35(26), pp. 7416–7428. doi: <https://doi.org/10.1016/j.biomaterials.2014.05.034>.
- Assmann, A. *et al.* (2017) 'Improvement of the in vivo cellular repopulation of decellularized cardiovascular tissues by a detergent-free, non-proteolytic, actin-disassembling regimen', *Journal of Tissue Engineering and Regenerative Medicine*, 11(12), pp. 3530–3543. doi: 10.1002/term.2271.
- Bobylev, D. *et al.* (2019) 'Double semilunar valve replacement in complex congenital heart disease using decellularized homografts', *Interactive Cardiovascular and Thoracic Surgery*, 28(1), pp. 151–157. doi: 10.1093/icvts/ivy212.
- Boethig, D. *et al.* (2019) 'A European study on decellularized homografts for pulmonary valve replacement: initial results from the prospective ESPOIR Trial and ESPOIR Registry data†', *European journal of cardio-thoracic surgery: official journal of the European Association for Cardio-thoracic Surgery*, 56(3), pp. 503–509. doi: 10.1093/ejcts/ezz054.
- Bonnet, Sébastien *et al.* (2007) 'A Mitochondria-K⁺ Channel Axis Is Suppressed in Cancer and Its Normalization Promotes Apoptosis and Inhibits Cancer Growth', *Cancer Cell*, 11(1), pp. 37–51. doi: 10.1016/j.ccr.2006.10.020.
- Bourget, J. M. *et al.* (2012) 'Human fibroblast-derived ECM as a scaffold for vascular tissue engineering', *Biomaterials*. Elsevier Ltd, 33(36), pp. 9205–9213. doi: 10.1016/j.biomaterials.2012.09.015.
- Brown, J. W. *et al.* (2011) 'Performance of SynerGraft decellularized pulmonary homograft in patients undergoing a Ross procedure', *Annals of Thoracic Surgery*. Elsevier Inc., 91(2), pp. 416–423. doi: 10.1016/j.athoracsur.2010.10.069.

- Cai, W. W. *et al.* (2009) 'Heparin coating of small-caliber decellularized xenografts reduces macrophage infiltration and intimal hyperplasia', *Artificial Organs*, pp. 448–455. doi: 10.1111/j.1525-1594.2009.00748.x.
- Carrabba, M. and Madeddu, P. (2018) 'Current Strategies for the Manufacture of Small Size Tissue Engineering Vascular Grafts', *Frontiers in Bioengineering and Biotechnology*, 6(April), pp. 1–12. doi: 10.3389/fbioe.2018.00041.
- Cartmill, T. B. (1987) 'Aorta-coronary bypass grafting with polytetrafluoroethylene conduits', *American Association for Thoracic Surgery*. American Association for Thoracic Surgery, 94(1), pp. 132–134. doi: 10.1016/S0022-5223(19)36328-7.
- Chan, A. H. P. *et al.* (2017) 'Evaluation of synthetic vascular grafts in a mouse carotid grafting model', *PLoS ONE*, 12(3), pp. 1–15. doi: 10.1371/journal.pone.0174773.
- Chen, Y. *et al.* (2017) 'Current advances in the development of natural meniscus scaffolds: innovative approaches to decellularization and recellularization', *Cell and Tissue Research*. Cell and Tissue Research, 370(1), pp. 41–52. doi: 10.1007/s00441-017-2605-0.
- Collins, M. J. *et al.* (2012) 'Therapeutic strategies to combat neointimal hyperplasia in vascular grafts', *Expert Review of Cardiovascular Therapy*, 10(5), pp. 635–647. doi: 10.1586/erc.12.33.
- 'Complementary Approaches : Dichloroacetate (DCA)' (2020), pp. 30–32.
- Copes, F. *et al.* (2019) 'Collagen-based tissue engineering strategies for vascular medicine', *Frontiers in Bioengineering and Biotechnology*, 7(JUL), pp. 1–15. doi: 10.3389/fbioe.2019.00166.
- Couet, F., Rajan, N. and Mantovani, D. (2007) 'Macromolecular biomaterials for scaffold-based vascular tissue engineering', *Macromolecular Bioscience*, 7(5), pp. 701–718. doi: 10.1002/mabi.200700002.
- Deuse, T. *et al.* (2014) 'Dichloroacetate prevents restenosis in preclinical animal models of vessel injury', *Nature*. doi: 10.1038/nature13232.
- Dong Wang (2015) *Individualized Cardiovascular Medicine: Identifying New Mechanisms to Inhibit the Development of Myointimal Hyperplasia Dissertation*. Universitätsklinikum Hamburg-Eppendorf .
- Duan, Y. *et al.* (2013) 'Antitumor activity of dichloroacetate on C6 glioma cell: In vitro and in vivo evaluation', *Oncotargets and Therapy*, 6, pp. 189–198. doi: 10.2147/OTT.S40992.
- Felden, L., Ku, D. N. and Chaikof, E. L. (2005) 'Mechanical Optimization of Vascular Bypass Grafts', *Building*, (May).
- Gauvin, R. *et al.* (2010) 'A novel single-step self-assembly approach for the fabrication of tissue-engineered vascular constructs', *Tissue Engineering - Part A*, 16(5), pp. 1737–1747. doi: 10.1089/ten.tea.2009.0313.
- Gelse, K., Poschl, E. and Aigner, T. (2003) 'Collagens--structure, function, and biosynthesis.', *Advanced drug delivery reviews*. Netherlands, 55(12), pp. 1531–1546. doi: 10.1016/j.addr.2003.08.002.
- Gilpin, A. and Yang, Y. (2017) 'Decellularization Strategies for Regenerative Medicine: From Processing Techniques to Applications', *BioMed Research International*. Hindawi, 2017. doi: 10.1155/2017/9831534.
- Gunatillake, P. A., Adhikari, R. and Gadegaard, N. (2003) 'Biodegradable synthetic polymers for tissue engineering', *European Cells and Materials*, 5, pp. 1–16. doi: 10.22203/eCM.v005a01.

- Hopkins, R. A. *et al.* (2014) 'Pulmonary arterioplasty with decellularized allogeneic patches', *Annals of Thoracic Surgery*, 97(4), pp. 1407–1412. doi: 10.1016/j.athoracsur.2013.12.005.
- James, M. O. and Stacpoole, P. W. (2016) 'Pharmacogenetic considerations with dichloroacetate dosing', *Pharmacogenomics*, 17(7), pp. 743–753. doi: 10.2217/pgs-2015-0012.
- Jones, S. G. *et al.* (2014) 'Stem cells accumulate on a decellularized arterial xenograft in vivo', *Annals of Thoracic Surgery*, 97(6), pp. 2104–2110. doi: 10.1016/j.athoracsur.2014.02.023.
- Kajbafzadeh, A. M. *et al.* (2017) 'Decellularization of Human Internal Mammary Artery: Biomechanical Properties and Histopathological Evaluation', *BioResearch Open Access*, 6(1), pp. 74–84. doi: 10.1089/biores.2016.0040.
- Kaplan, O. *et al.* (2017) 'Low-thrombogenic fibrin-heparin coating promotes in vitro endothelialization', *Journal of Biomedical Materials Research - Part A*, 105(11), pp. 2995–3005. doi: 10.1002/jbm.a.36152.
- Kelm, J. M. *et al.* (2010) 'A novel concept for scaffold-free vessel tissue engineering: Self-assembly of microtissue building blocks', *Journal of Biotechnology*. Elsevier B.V., 148(1), pp. 46–55. doi: 10.1016/j.jbiotec.2010.03.002.
- Khan, A., Andrews, D. and Blackburn, A. C. (2016) 'Long-term stabilization of stage 4 colon cancer using sodium dichloroacetate therapy', *World Journal of Clinical Cases*, 4(10), p. 336. doi: 10.12998/wjcc.v4.i10.336.
- Kho, A. R. *et al.* (2019) 'The Effects of Sodium Dichloroacetate on Mitochondrial Dysfunction and Neuronal Death Following Hypoglycemia-Induced Injury', *Cells*, 8(5), p. 405. doi: 10.3390/cells8050405.
- Koch, S. *et al.* (2010) 'Fibrin-poly lactide-based tissue-engineered vascular graft in the arterial circulation', *Biomaterials*, 31(17), pp. 4731–4739. doi: 10.1016/j.biomaterials.2010.02.051.
- Koens, M. J. W. *et al.* (2010) 'Controlled fabrication of triple layered and molecularly defined collagen/elastin vascular grafts resembling the native blood vessel.', *Acta biomaterialia*. England, 6(12), pp. 4666–4674. doi: 10.1016/j.actbio.2010.06.038.
- Kurniawan, H. (2019) 'Perfusion 3D Bioprinting with Gelatin and Hydrogel for Vascular Tissue Engineering', pp. 1–14. doi: 10.31224/osf.io/c7hsj.
- L'Heureux, N. *et al.* (1998) 'A completely biological tissue-engineered human blood vessel', *FASEB Journal*, 12(1), pp. 47–56. doi: 10.1096/fasebj.12.1.47.
- Lemson, M. S. *et al.* (2000) 'Intimal hyperplasia in vascular grafts', *European Journal of Vascular and Endovascular Surgery*, 19(4), pp. 336–350. doi: 10.1053/ejvs.1999.1040.
- Lin, C. H. *et al.* (2018) 'In vivo performance of decellularized vascular grafts: A review article', *International Journal of Molecular Sciences*, 19(7). doi: 10.3390/ijms19072101.
- Lindsey, P. *et al.* (2018) 'Lower Extremity Bypass Using Bovine Carotid Artery Graft (Artegraft): An Analysis of 124 Cases with Long-Term Results', *World Journal of Surgery*. Springer International Publishing, 42(1), pp. 295–301. doi: 10.1007/s00268-017-4161-x.
- Lisa M. Maurer, Ma, W. and Mosher, D. F. (2015) 'Dynamic Structure of Plasma Fibronectin', *Crit Rev Biochem Mol Biol.*, 51(4), pp. 213–227. doi: 10.1080/10409238.2016.1184224.

- Liu, X. *et al.* (2013) 'Aortic valve replacement with autologous pericardium: Long-term follow-up of 15 patients and in vivo histopathological changes of autologous pericardium', *Interactive Cardiovascular and Thoracic Surgery*, 16(2), pp. 123–128. doi: 10.1093/icvts/ivs441.
- Lovett, M. *et al.* (2010) 'Tubular silk scaffolds for small diameter vascular grafts', *Organogenesis*, 6(4), pp. 217–224. doi: 10.4161/org.6.4.13407.
- Mallis, P. *et al.* (2014) 'Evaluation of decellularization in umbilical cord artery', *Transplantation Proceedings*. Elsevier Inc., 46(9), pp. 3232–3239. doi: 10.1016/j.transproceed.2014.10.027.
- Marangos, P. J. *et al.* (1999) 'Dichloroacetate and cerebral ischaemia therapeutics', *Expert Opinion on Investigational Drugs*. Taylor & Francis, 8(4), pp. 373–382. doi: 10.1517/13543784.8.4.373.
- Marelli, B. *et al.* (2010) 'Compliant electrospun silk fibroin tubes for small vessel bypass grafting', *Acta Biomaterialia*. Acta Materialia Inc., 6(10), pp. 4019–4026. doi: 10.1016/j.actbio.2010.05.008.
- Matsuzaki, Y. *et al.* (2019) 'The Evolution of Tissue Engineered Vascular Graft Technologies: From Preclinical Trials to Advancing Patient Care', *Applied Sciences*, 9(7), p. 1274. doi: 10.3390/app9071274.
- McClure, M. J., Simpson, D. G. and Bowlin, G. L. (2012) 'Tri-layered vascular grafts composed of polycaprolactone, elastin, collagen, and silk: Optimization of graft properties.', *Journal of the mechanical behavior of biomedical materials*. Netherlands, 10, pp. 48–61. doi: 10.1016/j.jmbbm.2012.02.026.
- McKenna, K. A. *et al.* (2008) 'Mechanical Property Characterization of Electrospun Recombinant Human Tropoelastin for Vascular Graft Biomaterials Kathryn', *Bone*, 23(1), pp. 1–7. doi: 10.1038/jid.2014.371.
- McMurtry, M. S. *et al.* (2004) 'Dichloroacetate prevents and reverses pulmonary hypertension by inducing pulmonary artery smooth muscle cell apoptosis', *Circulation Research*, 95(8), pp. 830–840. doi: 10.1161/01.RES.0000145360.16770.9f.
- Michelakis, E. D. *et al.* (2015) 'Role of Increased Expression and Activity of Voltage-Gated Potassium Channels', pp. 244–251.
- Michelakis, E. D., Webster, L. and Mackey, J. R. (2008) 'Dichloroacetate (DCA) as a potential metabolic-targeting therapy for cancer', *British Journal of Cancer*, 99(7), pp. 989–994. doi: 10.1038/sj.bjc.6604554.
- Mills, B., Robb, T. and Larson, D. F. (2012) 'Intimal hyperplasia: Slow but deadly', *Perfusion (United Kingdom)*, 27(6), pp. 520–528. doi: 10.1177/0267659112452316.
- Mosher, D. F. (1993) 'Assembly of fibronectin into extracellular matrix', *Current Opinion in Structural Biology*, 3(2), pp. 214–222. doi: 10.1016/S0959-440X(05)80155-1.
- Nemes, A. *et al.* (1985) 'Application of a vascular graft material (Solcograft®-P) in experimental surgery', *Biomaterials*, 6(5), pp. 303–311. doi: 10.1016/0142-9612(85)90086-9.
- Niklason, L. E. *et al.* (1999) 'Functional arteries grown in vitro', *Science*, 284(5413), pp. 489–493. doi: 10.1126/science.284.5413.489.
- Niklason, L. E. *et al.* (2001) 'Morphologic and mechanical characteristics of engineered bovine arteries', *Journal of Vascular Surgery*, 33(3), pp. 628–638. doi: 10.1067/mva.2001.111747.

- Norotte, C. *et al.* (2009) 'Scaffold-free vascular tissue engineering using bioprinting', *Biomaterials*, 30(30), pp. 5910–5917. doi: 10.1016/j.biomaterials.2009.06.034.
- Pashneh-Tala, S., MacNeil, S. and Claeysens, F. (2016) 'The tissue-engineered vascular graft - Past, present, and future', *Tissue Engineering - Part B: Reviews*, 22(1), pp. 68–100. doi: 10.1089/ten.teb.2015.0100.
- Potts, J. R. (1975) 'Structure and Assembly', *Structure and Assembly*, pp. 648–655. doi: 10.1007/978-1-4684-2709-7.
- Ramalanjaona, G. R. *et al.* (1986) 'Fibronectin coating of an experimental PTFE vascular prosthesis', *Journal of Surgical Research*, 41(5), pp. 479–483. doi: 10.1016/0022-4804(86)90165-4.
- Ravi, S. and Chaikof, E. L. (2010) 'Biomaterials for vascular tissue engineering', *Regenerative Medicine*, 5(1), pp. 107–120. doi: 10.2217/rme.09.77.
- Rodríguez-Rodríguez, V. E. *et al.* (2018) 'Human umbilical vessels: Choosing the optimal decellularization method', *ASAIO Journal*, 64(5), pp. 575–580. doi: 10.1097/MAT.0000000000000715.
- Rosenberg, N. *et al.* (1966) 'Tanned collagen arterial prosthesis of bovine carotid origin in man. Preliminary studies of enzyme-treated heterografts.', *Annals of Surgery*, 164(2), pp. 247–256. doi: 10.1097/00006534-196703000-00052.
- Schmidli, J. *et al.* (2004) 'Bovine mesenteric vein graft (ProCol) in critical limb ischaemia with tissue loss and infection', *European Journal of Vascular and Endovascular Surgery*, 27(3), pp. 251–253. doi: 10.1016/j.ejvs.2003.12.001.
- Schwarzbauer, J. E. and DeSimone, D. W. (2011) 'Fibronectins, their fibrillogenesis, and in vivo functions', *Cold Spring Harbor Perspectives in Biology*, 3(7), pp. 1–19. doi: 10.1101/cshperspect.a005041.
- Simbara *et al.* (2017) 'A review on fibrous scaffolds in cardiovascular tissue engineering.', *Innovative Biomedical Technologies and Health Care (IBTHC)*, *Open Acces.[online]*, 1(1), pp. 14–28. Available at: <https://applispublishers.com/wp-content/uploads/2016/07/IBTHC-01-000104.pdf>.
- Song, H. G. *et al.* (2019) 'promise', 22(3), pp. 340–354. doi: 10.1016/j.stem.2018.02.009.Vascular.
- Song, R. *et al.* (2018) 'Current development of biodegradable polymeric materials for biomedical applications', *Drug Design, Development and Therapy*, 12, pp. 3117–3145. doi: 10.2147/DDDT.S165440.
- Stacpoole, P. W. *et al.* (1998) 'Clinical pharmacology and toxicology of dichloroacetate', *Environmental Health Perspectives*, 106(SUPPL. 4), pp. 989–994. doi: 10.1289/ehp.98106s4989.
- Stacpoole, P. W., Gilbert, L. R., *et al.* (2008) 'Evaluation of long-term treatment of children with congenital lactic acidosis with dichloroacetate', *Pediatrics*, 121(5). doi: 10.1542/peds.2007-2062.
- Stacpoole, P. W., Kurtza, T. L., *et al.* (2008) 'Role of Dichloroacetate in the Treatment of Genetic Mitochondrial Diseases', *Advanced Drug Delivery Reviews*, 60(13–14), pp. 1478–1487. doi: 10.1016/j.addr.2008.02.014.
- Sugimura, Y. *et al.* (2020) 'Controlled autologous recellularization and inhibited degeneration of decellularized vascular implants by side-specific coating with stromal cell-derived factor 1 α and fibronectin', *Biomedical Materials (Bristol)*. IOP Publishing, 15(3). doi: 10.1088/1748-605X/ab54e3.

- Tataranni, T. and Piccoli, C. (2019) 'Dichloroacetate (DCA) and Cancer: An Overview towards Clinical Applications', *Oxidative Medicine and Cellular Longevity*, 2019. doi: 10.1155/2019/8201079.
- Thomas, S. R. *et al.* (1991) 'Longterm study of a compliant biological vascular graft', *European Journal of Vascular Surgery*, 5(2), pp. 149–158. doi: 10.1016/S0950-821X(05)80680-2.
- Tillman, B. W. *et al.* (2009) 'The in vivo stability of electrospun polycaprolactone-collagen scaffolds in vascular reconstruction', *Biomaterials*. Elsevier Ltd, 30(4), pp. 583–588. doi: 10.1016/j.biomaterials.2008.10.006.
- To, W. S. and Midwood, K. S. (2011) 'Plasma and cellular fibronectin: Distinct and independent functions during tissue repair', *Fibrogenesis and Tissue Repair*. BioMed Central Ltd, 4(1), p. 21. doi: 10.1186/1755-1536-4-21.
- Toshmatova, M. *et al.* (2019) 'Influence of laminin coating on the autologous in vivo recellularization of decellularized vascular prostheses', *Materials*, 12(20). doi: 10.3390/ma12203351.
- Udelsman, B. V, Maxfield, M. W. and Breuer, C. K. (2013) 'Tissue engineering of blood vessels in cardiovascular disease: moving towards clinical translation', *Heart*, 99(7), pp. 454 LP – 460. doi: 10.1136/heartjnl-2012-302984.
- Van Uden, S. *et al.* (2019) 'A novel hybrid silk-fibroin/polyurethane three-layered vascular graft: Towards in situ tissue-engineered vascular accesses for haemodialysis', *Biomedical Materials (Bristol)*. IOP Publishing, 14(2). doi: 10.1088/1748-605X/aafc96.
- Virani, S. S. *et al.* (2020) *Heart disease and stroke statistics—2020 update: A report from the American Heart Association*, *Circulation*. doi: 10.1161/CIR.0000000000000757.
- Wang, C. *et al.* (2010) 'A small diameter elastic blood vessel wall prepared under pulsatile conditions from polyglycolic acid mesh and smooth muscle cells differentiated from adipose-derived stem cells', *Biomaterials*. Elsevier Ltd, 31(4), pp. 621–630. doi: 10.1016/j.biomaterials.2009.09.086.
- Wang, L. *et al.* (2015) 'Decreasing mitochondrial fission diminishes vascular smooth muscle cell migration and ameliorates intimal hyperplasia', *Cardiovascular Research*, 106(2), pp. 272–283. doi: 10.1093/cvr/cvv005.
- Wilshaw, S. P. *et al.* (2012) 'Development and characterization of acellular allogeneic arterial matrices', *Tissue Engineering - Part A*, 18(5–6), pp. 471–483. doi: 10.1089/ten.tea.2011.0287.
- Wise, S. G. *et al.* (2011) 'A multilayered synthetic human elastin/polycaprolactone hybrid vascular graft with tailored mechanical properties', *Acta Biomaterialia*, 7(1), pp. 295–303. doi: 10.1016/j.actbio.2010.07.022.
- World Health Organisation (2017) *Cardiovascular Diseases*. Available at: https://www.who.int/health-topics/cardiovascular-diseases/#tab=tab_1.
- Wystrychowski, W. *et al.* (2014) 'First human use of an allogeneic tissue-engineered vascular graft for hemodialysis access', *Journal of Vascular Surgery*. Society for Vascular Surgery, 60(5), pp. 1353–1357. doi: 10.1016/j.jvs.2013.08.018.
- Zhao, H. *et al.* (2019) 'Sodium dichloroacetate stimulates angiogenesis by improving endothelial precursor cell function in an AKT/GSK-3 β /Nrf2 dependent pathway in vascular dementia rats', *Frontiers in Pharmacology*, 10(MAY). doi: 10.3389/fphar.2019.00523.
- Zhao, Y. *et al.* (2020) 'Small rodent models of atherosclerosis', *Biomedicine and Pharmacotherapy*. Elsevier, 129(April), p. 110426. doi: 10.1016/j.biopha.2020.110426.

ACKNOWLEDGMENT

I want to thank all the people who have helped me work toward this thesis:

First, I would like to thank my supervisor, Prof. Dr. Alexander Assmann, for the thoughtful comments and recommendations on this dissertation. Throughout the writing of this dissertation, I have received a great deal of encouragement. Without his persistent help, the goal of this project would not have been realized.

Furthermore, I would like to express my special gratitude to Prof. Dr. Artur Lichtenberg, head of the department for cardiac surgery, and Prof. Dr. Payam Akhyari, the deputy director of the clinic for cardiac surgery and the head of the research group for experimental surgery, for the opportunity to be part of the research group and for your trust. You supported me greatly and were always willing to help me.

I want to acknowledge all scientific staff, including the research assistants and postdocs at the clinic for cardiovascular surgery, for the laboratory training and support in conducting the tests.

I wish to acknowledge the German Academic Exchange Service (DAAD) for financial support and for enabling me to complete my doctoral degree in Germany. This dissertation would not have been possible without funding.

To conclude, I cannot forget to thank my family. I am grateful to them for encouraging me in all of my pursuits and inspiring me to follow my dreams. I am especially grateful to my mother, who supported me emotionally. I always knew that she believed in me and wanted the best for me.